Recent trends of silicon elastomer-based nanocomposites and their sensing applications

Gulshan Verma, Nikhil Sheshkar, Chandan Pandey, Ankur Gupta*
Department of Mechanical Engineering, Indian Institute of Technology Jodhpur-342037, India
*Corresponding author: ankurgupta@iitj.ac.in

Abstract

This paper reviews the various fabrication methodologies explored for the polydimethylsiloxane (PDMS) based nanocomposites along with their applications in sensing and other domains. PDMS is well known for its biocompatibility, durability, transparency, and adoptability to any size and shape via replication technique. Envisioning its potential and prospects in flexible device realization, this review discusses various methods used by researchers to develop PDMS-based nanocomposites and approaches to improve their functional properties along with their associated applications. This review article aims to provide insights into the state-of-the-art work carried out in this province which will certainly be helpful for researchers of a similar field.

Keywords: PDMS, silicon elastomer, polymer base composites.

1 Introduction

Technological innovations have raised the level of current microfabrication approaches to develop affordable, compact, and efficient systems and devices. These devices have enormous applications in diversified domains such as microfluidics, biomedical, sensing, communication, tissues engineering so and so forth. In the miniaturized domain, selective substrates have been known to be utilized such as Si, glass, and certain distinct class of polymers [1–3]. Usage of the polymers arises due to some dimensional and functional constraints in the hard substrates viz. Si, glass, etc. Among various fabrication approaches in micro and nanotechnology viz., photolithography, sputtering, molecular beam epitaxy, chemical/physical vapor deposition, and many more, there are a few options available when it comes to fabricating flexible/stretchable functional devices [4–9]. To date, various polymers such as polycarbonate, polyimides, polyurethane, polymethyl methacrylate, polystyrene, polydimethylsiloxane (PDMS), and other prepolymers have been explored for flexible device manufacturing. Soft polymers, such as polydimethylsiloxane (PDMS), are very flexible and may be structured to the required dimensions, especially by integrating nanoparticles to produce smart materials, which has gained attention in microfluidic systems and sensing technologies[10, 11]. Due to the two dimensions of homogeneity and stability, the process of synthesizing such nanocomposite-based PDMS nanocomposite is significantly difficult. From the past few years, the main research continues to focus on coordinating the needed processing stages, which is critical for developing better, smarter, and more sensitive materials for high-performance sensing applications. The choice of nanoparticles in the polymer matrix helps to improve the conductivity of the insulating polymer and changes in different electrical characteristics of the material impacted by external physical or chemical changes. PDMS is a non-conductive silicone-based elastomer that has been utilized for over a decade for fast prototyping microdevices for various sensing

applications[12–17]. Table 1 describes several polymer materials and their characteristics. PDMS, for example, is widely known in the realm of polymer science and has been intensively researched for the flexible device[18–21]. Similar nanocomposites have been studied by a number of researchers for various sensing applications[22–28]. Figure 1 depicts the number of research completed in the field of PDMS-based nanocomposites and associated applications during the last 20 years.

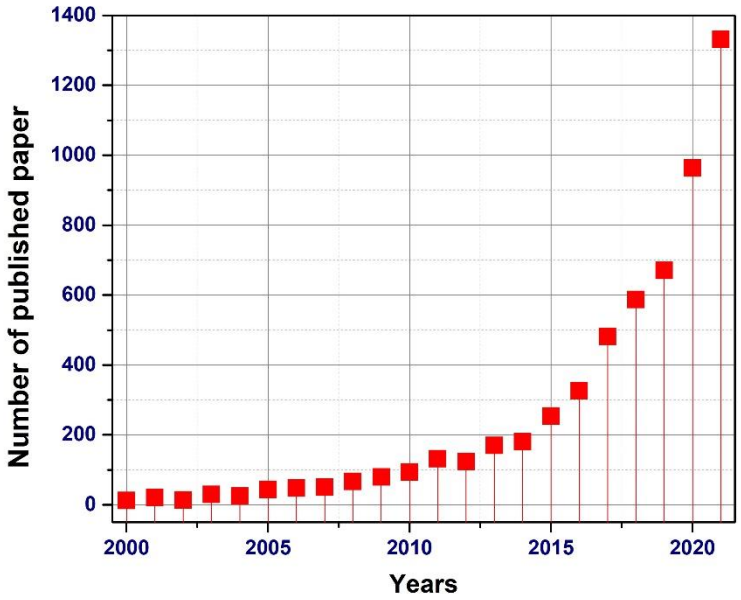

Figure 1. Graph showing the variation in a paper published in the past two decades.

Table 1. Polymers used for microfabrication and their properties[29–32].

Polymers	**Density**	**Transmittance**	**Toughness and Tensile Strength**	**Refractive index**	**Chemical Resistance**	**Heat Resistance**	**Application**
Polycarbonate	1.27 to 1.38 g/cm^3	Able to transmite 90% of light	Toughness =6.683 MPa.m$^{1/2}$ Strength = 165 MPa	1.584	Good chemical resistance against diluted acids, aliphatic hydrocarbons, and alcohols	Thermally stable up to 135˚C	safety helmets, bullet-proof glass, car headlamp lenses, baby feeding bottles
Polyimides	1.31 to 1.43 g/cm^3	Transparent in nature	Toughness = 60-112 J/m Strength = 120 MPa	1.50	Good chemical resistance to acetone, benzene, ethanol, and kerosene	Thermally stable < 500˚C	aerospace and automotive industry
Polyurethane	1.22 to 1.27 g/cm^3	Generally Opaque.		1.52 to 1.57 (TPU)	Chemical property depends on types of isocyanates and polyols used to make it	Can be used in the temperature range of -62˚ C to 93˚C	Synthetic fibers, Carpet underlay

Polymethyl methacrylate	1.17 to 1.20 g/cm^3	Able to transmite 92% of light	Toughness = 2.26 MPa. m$^{1/2}$ Strength = 75 MPa	1.49	susceptible to organic solvent attacks	Thermally stable up to 80˚C	car windows, LCD/LED tv screens, drug testing devices
Polystyrene	0.96 to 1.05 g/cm^3	Excellent	Toughness = 15 to 20 J/m Strength = 75 MPa	1.6	Good chemical resistance to diluted acid and bases.	Thermally stable up to 249˚C	General household appliance, packaging, toys, beakers

Although PDMS has poor chemical compatibility and low hardness due to which it has restrictions in some chemical and high-pressure applications, it has additional advantages in terms of its visibility, capability to be molded to any 2-, 3- dimensional features.

2 Fabrication Methodology using PDMS

Nanomaterials are often embedded, deposited, and mixed with PDMS to regulate or modify the distinctive characteristics of PDMS in order to develop PDMS-based nanocomposite devices. Nanostructures can also be printed on PDMS to produce nanopillars and nano-porous films. The fabrication of PDMS-based nanocomposite materials for a range of sensor-based applications is described in this section. Among various fabrication techniques available in microfabrication, photolithography [33, 34] is one of the widely used processes. Designing and manufacturing of micro-level features require photolithography followed by an etching process which offers great advantages in silicon based micro-electronics and micro-electromechanical systems[35–39]. The drawback of photolithography is that it can be used for flat surface application only and it has minimum feature size constraint i.e. it is difficult to manufacture the patterns less than 100 nm[40–43]. To overcome the drawback of hard substrate-based photolithography, another method is explored which is known as “soft lithography”. This method is a simpler and cheaper alternative to conventional photolithography. In this technique, patterns are created on microchips using replica molding. This same pattern is transferred from the master to the elastomer after treatment or solidification. There are different applications of soft lithography and accordingly different micro fabrication techniques. Herein, a summary of six different methods is discussed below[44].

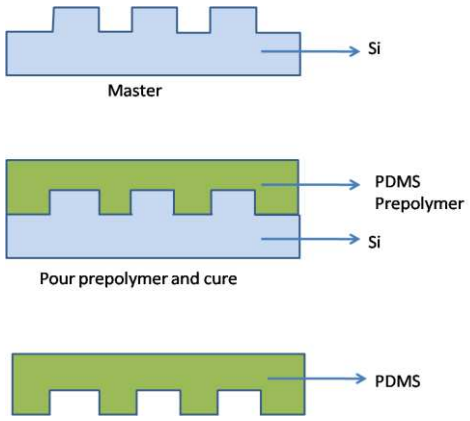

Figure 2. Steps to manufacture stamp.

In this technique, PDMS and curing agents were generally mixed in a ratio of 10:1 and then poured into the silicon master. Liquid PDMS take shape of a master and then is heated to provide strength by cross-linking. This element is also known as a stamp (see figure. 2).

A. Micro contact printing

PDMS stamp is used and ink (solution of $CH_3(CH_2)15SH$ in ethanol) is applied to it using a cotton swab. Then stamp is placed over a metal-coated silicon substrate. A layer of metal comes in contact with the stamp and takes its shape. The stamp is removed from the metal layer after 10 to 20 s [45]. We get the monolayer of alkanethiol on the silicon substrate (see figure 3(a))**.**

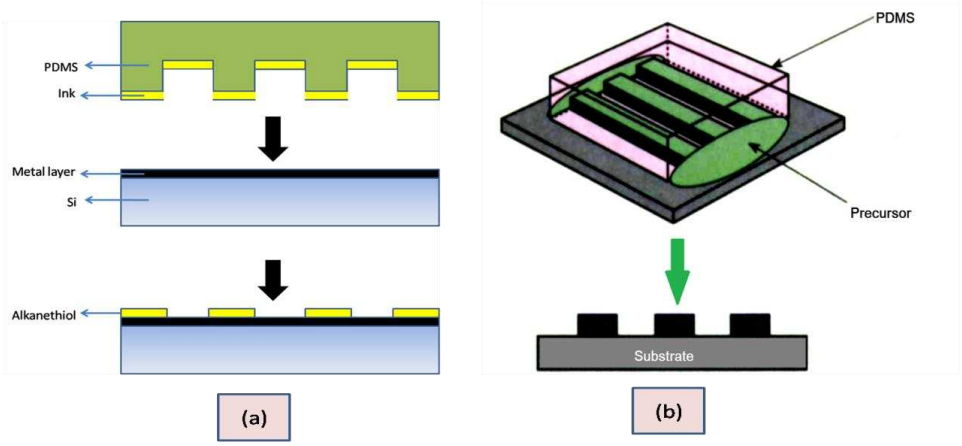

Figure 3 (a) Diagram showing Steps for micro contact printing (b) Diagram showing micro moulding in capillaries

B. Micro moulding in capillaries

Connected channels are mounted on a substrate that is connected to a PDMS mould. In the channels, capillary action takes place, a low viscous liquid drops at one end and comes up due to capillary action[46, 47]. The interconnected system is then heated to form a channel in PDMS. Mold can be removed thereafter (See figure 3(b)). This method has been used to structure a variety of materials, including polymers, prepolymers, proteins, sol-gel precursors and colloids. It also includes microfluidic and nanofluidic technologies for the production of biochemical devices[48, 49]. Kim et al. devised a method for forming capillary channels between an elastomeric PDMS foam and a support. The low reactivity of PDMS makes it easier to detach from the microstructure on the substrate, and its compliant nature facilitates conformal contact between the mould and the substrate. The elastomeric component is removed when the organic or inorganic substance in the liquid polymerizes/crystallizes, attaches/adsorbs, or interacts with the substrate's surface, and the pattern of the material remains on the substrate. As a result, the master pattern is repeated in a structure that extends to the substrate's surface [47].

C. Micro transfer Moulding

PDMS stamp is poured by a small liquid drop of the prepolymer. The excess prepolymer is wiped out and the filled mould is placed on the substrate[50]. Now heat the system and then separate the mould and substrate, prepolymer remains on the substrate (see figure 4a). The method of micro transfer moulding has a number of major advantages. The entire procedure is fast, with microstructures being replicated in less

than four minutes. Structures made of two materials (such as, polymer doped dye) can be manufactured with a homogeneous concentration of the dopant throughout the pattern using micro transfer moulding. This process is also less susceptible to fluctuations in prepolymer viscosity during the process because of the fast speed of the process. Micro transfer has the added benefit of being able to work with a wide range of materials [51]. In another study, a MEMS chip was packed using the PDMS micro-transfer mould process to assess the interconnection performance in a PCB board[52].

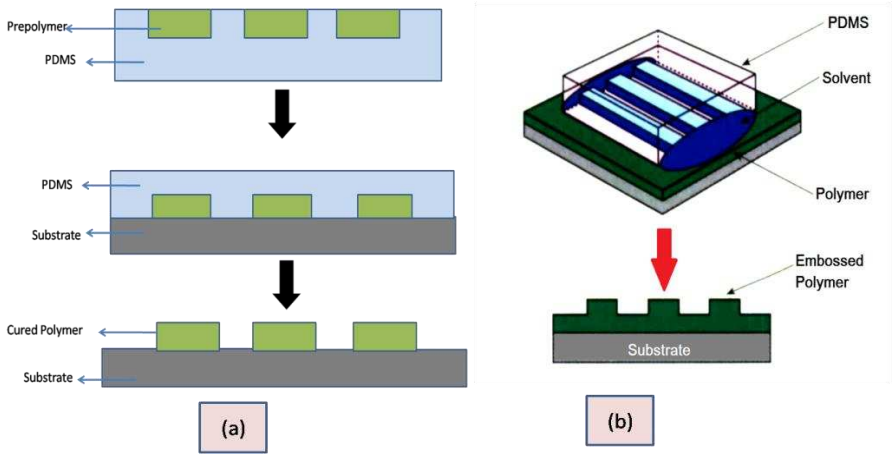

Figure 4. (a) Fabrication using micro-transfer molding (b) Solvent assisted micro moulding

D. Solvent assisted micro moulding (SAMIM)

The liquid Solvent of polymer is filled in the PDMS mould. The substrate with a thin film of polymer comes in contact with PDMS mould, polymer dissolves in a solvent. This results in taking shape of mould[53]. The mould is left till the solvent gets evaporated for some time and then separates from the substrate(see figure 4b). The patterned surface becomes a replica of the PDMS mould surface after the solvent evaporates. the solvent should be selected in such a manner that the PDMS mould do not get damaged. Solvent has to evaporate quickly, thus solvents with a high vapor pressure are ideal for this. A pre-treatment to make the PDMS surface hydrophilic is usually used when utilizing solvents that do not wet the PDMS surface, such as water. Unlike MIMIC, this approach creates features that are interconnected by a residual layer. The period of contact of the mould can affect the capillary rise of the material when softened with the solvent[54].

E. Replica moulding

Precursor polyurethane is coated on PDMS. Polyurethane is separated from the mould after heating in presence of UV light, which gives a replica of the master[55]. Figure 5, shows the schematic of replica moulding and near field contact mode lithography.

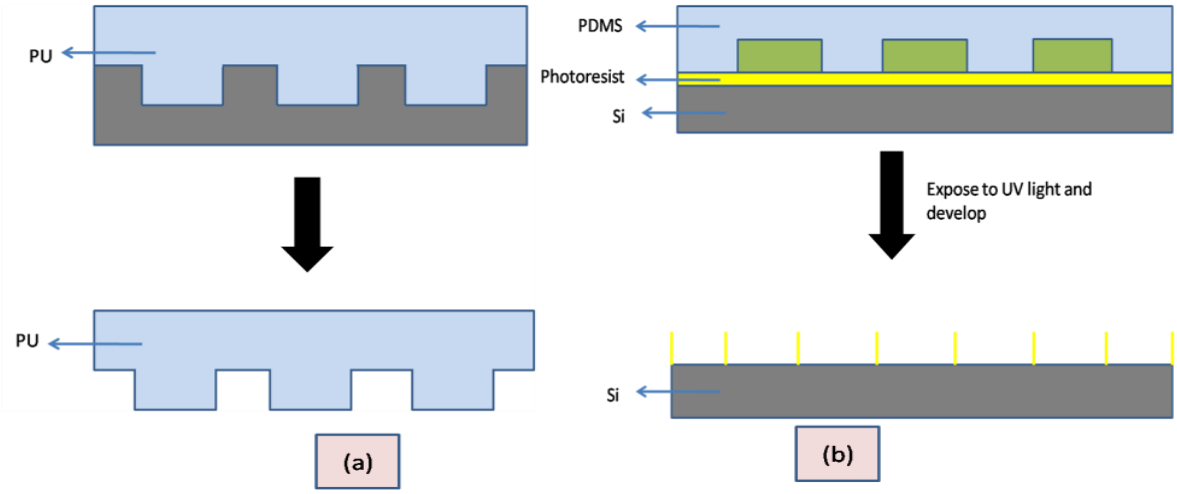

Figure 5. Diagram showing (a) Replica moulding (b) Near field contact mode lithography.

F. Near field contact mode lithography

In this process, a photoresist material is exposed to Ultraviolet light through a mask. The exposed photoresist material gets dissolved and takes a shape of a mask (about 100nm)[56]. The resolution of contact mode lithography is dependent on the wavelength of light and photoresist's refractive index. When refractive indexes are increases the resolution is enhanced, which is feasible than reducing the wavelength of light[57]. Paik et al. present a technology that employs a photomask made of Cr patterns implanted in an elastomeric mask plate to provide a simple and powerful lithographic approach. Because of its near-field alignment with the surface, it enables for the production of feature sizes below the diffraction limit of light. Mechanically stable soft photomasks give great resolution and outstanding dependability even on a highly curved surface when combined with near-field capabilities for sub-wavelength feature production[58].

In the next section, different methods of fabrication of PDMS nanocomposites and the associated change in the properties of PDMS are discussed. This improvised property leads to the application of PDMS in different fields.

2.1 Various fabrication techniques

2.1.1 Solvent-Assisted Nanoparticle Deposition

The most common method for depositing nanoparticles on PDMS is to use a sputtering and e-beam evaporator under dry environments. These procedures, on the other hand, need costly multi-step equipment such as photoresist lithography, etching, and lift-off operations. Solvent-assisted NP deposition, on the other hand, is a quick and easy way to make nanoparticles, permitting alterations to the whole surface of the PDMS [59]. Chen et al. [60] describe the manufacturing process for sandwich-like PDMS/CNTs/PDMS composites. Firstly, 0.04wt% CNT is mixed with propanol-2 and sprayed uniformly over the surface of polytetrafluoroethylene (PTFE) substrate. The internal content of a PDMS / CNT / PDMS composite was defined in this research using the areal density of CNTs. Spray times can be used to alter the CNT content. Meanwhile, the viscosity of the prepolymer PDMS was reduced by diluting it with a xylene 1:1 ratio, then combining it with the curing agent at a 10: 1 ratio for 30 minutes with stirring. The PDMS solution (diluted) was then placed over a CNT-coated PTFE substrate and let to evaporate the xylene solvent fully for 24

hours. The CNT-carrying PDMS film is cured for 35 minutes at 100° C, before being carefully peeled away from the PTFE substrate. The sample and the electrode are in close proximity. The conductive layer has a width of 0.6 cm and a distance of 2 cm between the two electrodes. To construct a sandwich-like structure, an additional layer of PDMS was cured, and the top surface of the CNT infiltration network was covered with Cu electrodes. Similarly, Solvent Assisted Nanoscale Embossing (SANE) was able to enhance pattern spacing by 100% and decrease it by 50%. Furthermore, by regulating and swelling the elastomer SANE type with a range of solvents, SANE was able to minimize the crucial structural size by up to 45 percent compared to the original master[61]. SANE is a nanofabrication process that can produce four classes of patterns from a single master. (a) A high-density array, (b) a low-density, (c) Various lattice symmetries, (d) arrays with smaller significant feature sizes with the same density as the previous two. As a result, SANE can create a huge number of novel templates and patterns that can be readily converted to functional materials and devices utilizing conventional production processes(see figure 6). Figure 7 shows the various methods for fabricating PDMS-based nanocomposites.

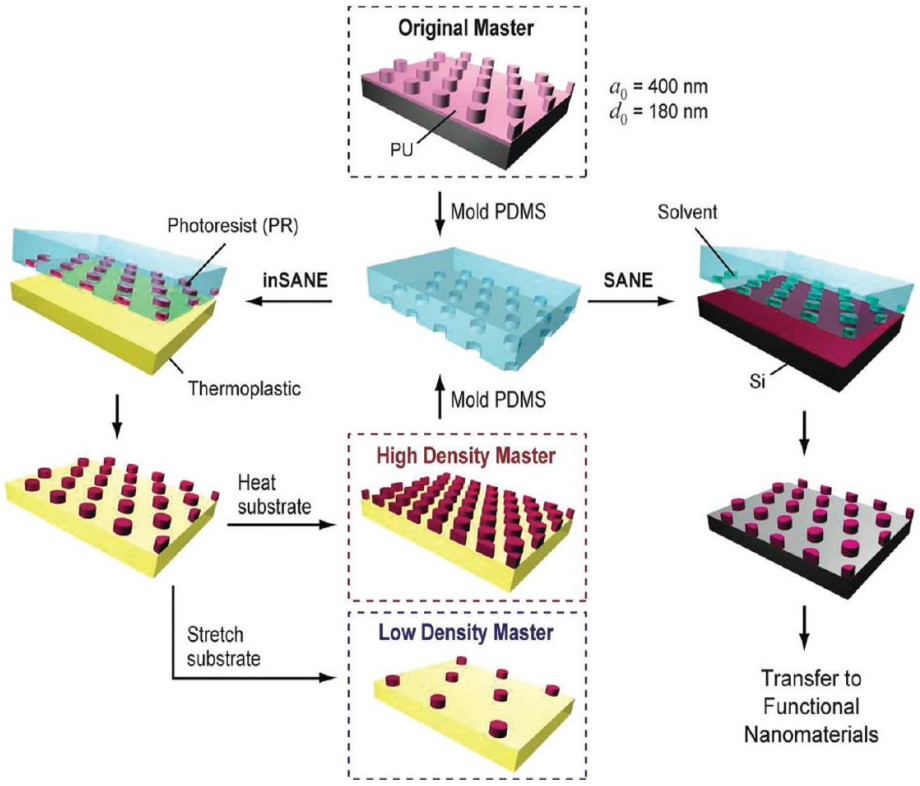

Figure 6. The schematic representation of the nanofabrication technique involves preparing low and high-density masters using the In-SANE technique. Reproduced with kind permission [61]).

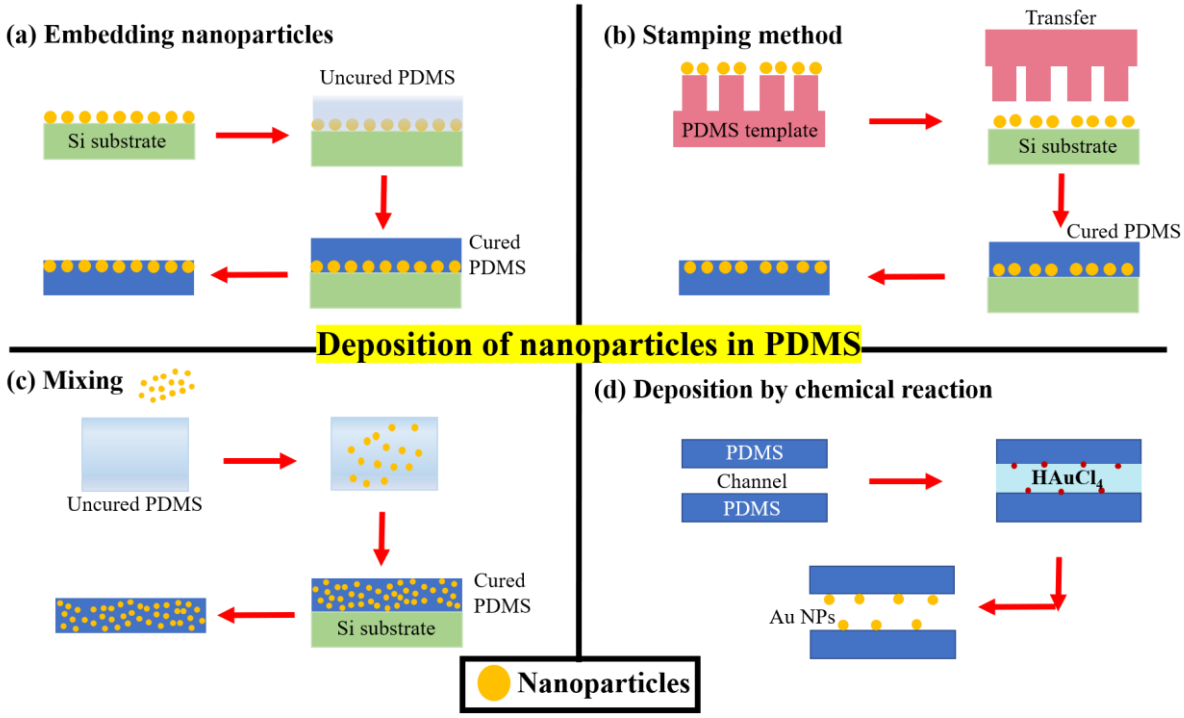

Figure 7. Various methods for preparing PDMS-based nanocomposite.

2.1.2 Ultrasonic wave treatment

PDMS-based nanocomposite may be easily made using mixing procedures. In contrast to CVD, the mixed technique allows the thermal, electrical, and mechanical characteristics of pure PDMS to be modified macroscopically [62]. PDMS nanocomposites may be created to modify the modulus of elasticity of pure PDMS, allowing changeable matrix stiffness [63]. A nanocomposite material with a modulus of 0.8 MPa is created when the volume ratio of silica NP to uncured PDMS is 1: 9. This is more than double the amount of native PDMS [62]. Metallic nanoparticles are commonly employed to change both structural and electrical characteristics. The elastic modulus of a 0.1 weight percent mixture of silver (Ag) NPs and PDMS is three times that of native PDMS [63]. Furthermore, the electrical conductivity of a mixture of Ag flakes and PDMS containing 8.6 wt. percent Ag was 5000, and the electrical conductivity of an Ag nanowires-PDMS mixture was around 8000 S/cm[64, 65]. CNTs have poor electrical conductivity when compared to metal nanomaterials. The PDMS-CNTs based composite, on the other hand, has better structural stability and may be used in applications such as flexible elastic batteries, flexible electronic skins, and many more[66]. Similarly, magnetic nanoparticles have the ability to transform magnetic energy into heat energy. The complex combination of PDMS and ferric oxide NP may create thermal energy at five different temperature increase rates when exposed to an alternating magnetic field [67]. The crystal structure of ferric oxide nanoparticles is related to an overall magnetic moment. The magnetic moment may be repeatedly disturbed or relaxed to create heat energy by introducing an external magnetic field [68].

Sun et al. reported the PDMS and multi-walled carbon nanotubes (MWCNT) based ultra-thin film. In this work, a two-step ultrasonication treatment technique was used to fabrication PDMS-based nanocomposite. MWCNT more than 10% gives a compact stack structure in the nanocomposites, which results in uniform electric heating and high thermal conductivity. This treatment helps in increasing the void space of

MWCNT to enhance the impregnation of PDMS in nano-paper(see figure8a). To prepare the nano-paper (NP), MWCNT 0.28 wt% and 0.82 wt % sodium dodecyl sulfate (SDS) was prepared in water and then subjected to Ultrasonic vibration for 4 hrs. Centrifugation at 4000 RPM for 8 min was done which help in removing large size particles. Polytetrafluoroethylene (PTFE) filtration membrane of size (25×30) cm was then used to perform vacuum filtration. After keeping it at room temperature for 0.5 h for drying, a thin film of MWCNT is obtained. After 3h in 125°C in a vacuum, nano-paper was achieved [69–72] Polydimethylsiloxane and the curing agent were mixed in a weight ratio of 10:1, and air bubbles were removed in the evacuating chamber. The mixture was then applied on both sides of the nano-paper prepared earlier. The ultrasonic wave was applied to the top surface of PDMS for 2 s at 2KW power. Now second ultrasonic treatment was done in the same liquid of PDMS when MWCNT/PDMS NC was transferred in it. For 0 to 100 s low power, ultrasonic waves were passed at room temperature(see figure 8b). Then roller was used to remove the excess PDMS. Then it was thermally cured in a vacuum oven for 2 h.

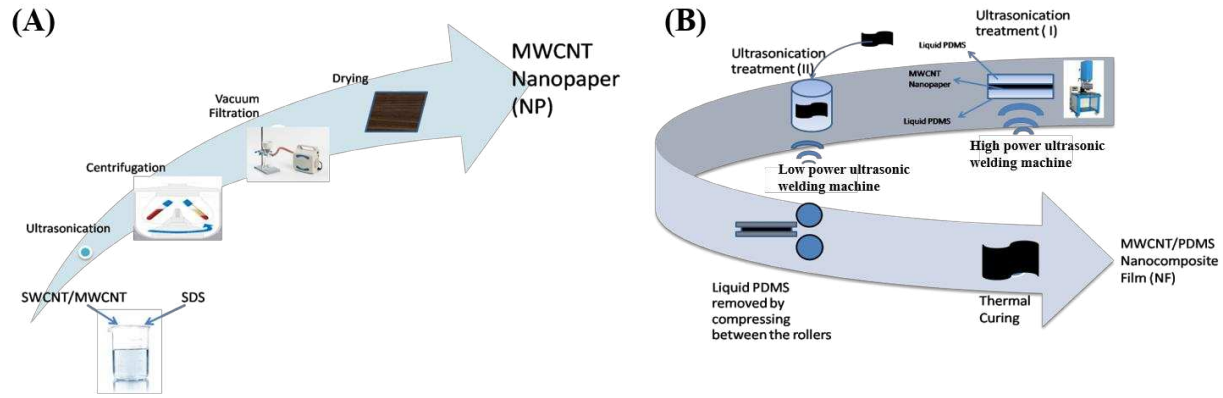

Figure 8. Two-step ultrasonication treatment (a) Manufacturing of MWCNT nano-paper (b) Manufacturing of MWCNT/PDMS Nanocomposite film.

2.1.3 Self-assembly approach

Cao et al. reported two approaches to construct graphene oxide i.e. sheet and nanoribbon. On adding less than 0.1 % by weight of two GO derivatives we get significant changes in flame retardancy and thermal stability of PDMS. PDMS-OH, PDMS-H, inhibitor, and water were mixed at 1000 rpm for 5 min[73, 74]. PDMS-Vi and catalyst were added to this mixture and were then poured into a mould and foamed for 15 min at room temperature[75]. The sample was then thermally cured by putting it into an oven at 100°C for 2 Hours[76–79]. Figure 9 shows the schematic for the preparation of SiRF nanocomposites.

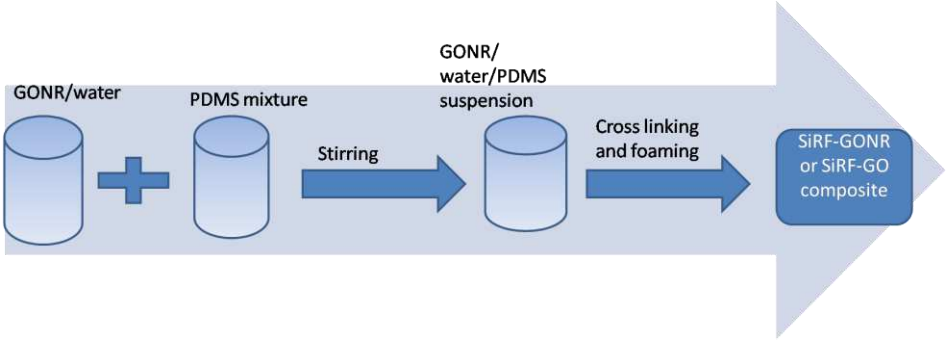

Figure 9. Manufacturing process of silicone rubber foam (SiRF) nanocomposites.

Wu et al. [80] described a new and easy approach for making a porous composite of PDMS/Carbon nanofiber using a standard dip-coating approach. Firstly, brown sugar granules are used as a template for producing a thin layer of pure and porous PDMS. Carbon nanofiber (CNF) was then applied to the porous PDMS by immersing it in a CNF dispersion in a GO-isopropyl alcohol solution, followed by drying in a vacuum oven. The porous PDMS was treated in an oxygen plasma chamber before dip coating. Figure 10 shows the preparation step and SEM images of PDMS/carbon nanofiber.

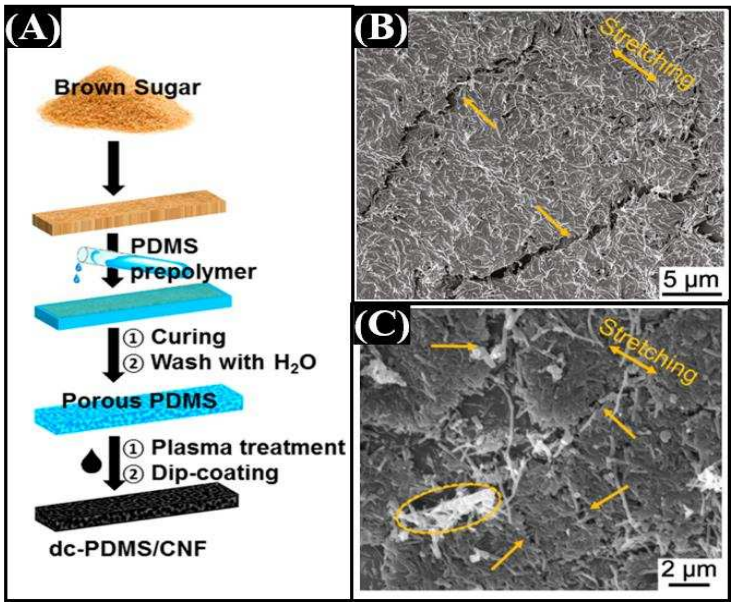

Figure 10. (A)Schematic representation of fabrication methodology used, (B-C) Typical SEM images for the dc-PDMS/CNF nanocomposites after being stretched between 0% and 30% for 200 cycles. (Reproduced with kind permission [80])

2.1.4 Embedding and Stamping Nanomaterials Onto PDMS

PDMS-based nanocomposites can also be produced by stamping and embedding nanoparticles s into the PDMS matrix. The production of aligned nanoparticle mono-layer and optically transparent layers suited for spectroscopic applications is possible using embedding procedures that inject nanoparticles s under the surface of PDMS. Monolayers of nanoparticles are often formed using stamping, Langmuir Blodgett (LB), and Layer-by-Layer (LBL) techniques[81]. A stamping procedure may be used to transfer an NP monomolecular layer from glass to a PDMS substrate, and these stacked nanoparticles layers can then be incorporated into PDMS. Deionized water deposition of positively charged Ag-NP resulted in a monomolecular layer of positively charged Ag- nanoparticles on the glass substrate. This layer adheres to the negatively charged glass surface electrostatically. After washing, the negatively charged Ag nanoparticles were immersed in deionized water to generate a second nanoparticles layer, resulting in a double layer of Ag NP. Immersion in water repeatedly results in an aligned Ag- nanoparticles multilayer. LB is another way of monolayer generation that relies on AuNP self-assembly at the water/hexane interface. When hexane is added to Au nanoparticles dissolved in Deionized water, the interface of hexane-water has high interfacial energy. Due to the anions of gold chloride and citrate, Au nanoparticles have a negative

surface charge in this state, and all Au nanoparticles s are distributed in the aqueous phase. The surface charge density of Au nanoparticles was dramatically lowered when ethanol was added to the solution for protonation. To maintain equilibrium, Au nanoparticles were relocated to the hexane-water contact. The electrostatic repulsion and van der Waals attraction of Au nanoparticles at the contact also resulted in a monomolecular layer of Au nanoparticles that was consistently aligned [82]. After hexane was evaporated, the Au-nanoparticle monolayer was floated on water and transferred to a wafer through a dipping and lifting procedure [83]. Following the fabrication of the Au-nanoparticle monomolecular layer, a PDMS and curing agent is mixed in 10:1 and poured on the substrate. The Au doped PDMS substrate may be simply removed from the substrate once the PDMS has cured. The stamping method is comparable to embedding technology in principle. A single layer of high-density nanoparticle was applied to a flat substrate, then transferred to a structured PDMS stamp, and ultimately printed onto the target substrate [84].

2.1.5 Electrospinning approaches to fabricate PDMS embedded nanofibers

Wang et al. reported PDMS with embedded electrospun nanofibers. This can be achieved by the solvent mixing process. On adding 0.5 wt % of both types (PAN and PVA), three times increase in adhesion strength can be achieved. Polyacrylonitrile (PAN)(8% weight) and polyvinyl alcohol (PVA)(10% weight) solution is made in dimethylformamide (DMF) and deionized water respectively [85, 86]. The electrospinning method is used in both cases in which the needle flow rate was 20 µl min^{-1} at a constant distance of 10 cm from the collector and syringe tip electrode, at 15 kV and 25 kV for PAN and PVA respectively [87, 88]. These fibers were then heated under vacuum at 2000 C[88]. Nanofibers produced were diffused in ethyl acetate and inserted in PDMS using the solution mixing method. Ultrasonication was done to stabilize the dispersion. Prepared dispersion and PDMS were added in the ratio of 0.3:1 and mixed for 1 h [89, 90]. Now the mixture was kept at 550˚C to remove the solvent completely and a cross-linking agent was added[91–94]. After removing the trapped gases in the vacuum chamber, the suspension was then placed between two glass slides. The glass slide was kept in an oven at 100°C for 2 h. This results in an improvement in cohesive strength[87, 95–97]. Figure 11 shows various steps involve in preparing PDMS embedded PAN and PVA nanofibers.

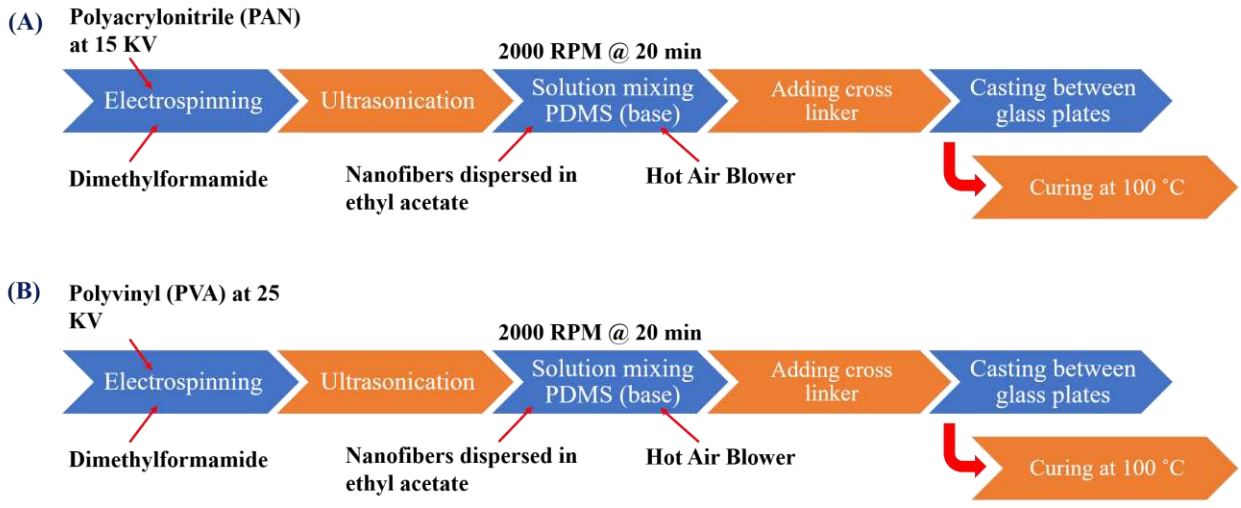

Figure 11. (a) Steps for preparing PAN fiber/PDMS composite (b) Steps for preparing PVA fiber/PDMS composite

Wang et al. [98] fabricated a conductive composite by ultrasonically doping CNTs on the surface of thermoplastic polyurethane nanofibers and then coating them with PDMS. Figure 12 shows the schematic of the fabrication step and SEM images of the prepared composite. Firstly, pallets of thermoplastic polyurethane were mixed with a THF/DMF solution (1:3) and magnetically stir for 12 hours at 60° C, to obtain a uniform TPU solution having a concentration of 14% by weight. The TPU solution was then injected into a syringe and pushed out at a rate of 1.1 mL/h through a nozzle connected to a high voltage power supply. The CNTs were then ultrasonicated for 30 minutes in ethanol to get a properly distributed CNT solution. The membrane of TPU fibers was then inserted into the CNT solution. The CNTs progressively rooted themselves to the surface of nanofibers during ultrasonication. Finally, the CNT-doped nanofiber was washed multiple times with deionized water to eliminate impurities before being heated in an oven at 60°C for 6 hours. The PDMS solution was made by combining the PDMS elastomer and the curing agent in hexane in the ratio of 10:1. The CNT-doped nanofiber was then submerged in PDMS solution and placed in an oven for 2 hours at 80 °C to obtain the final composite.

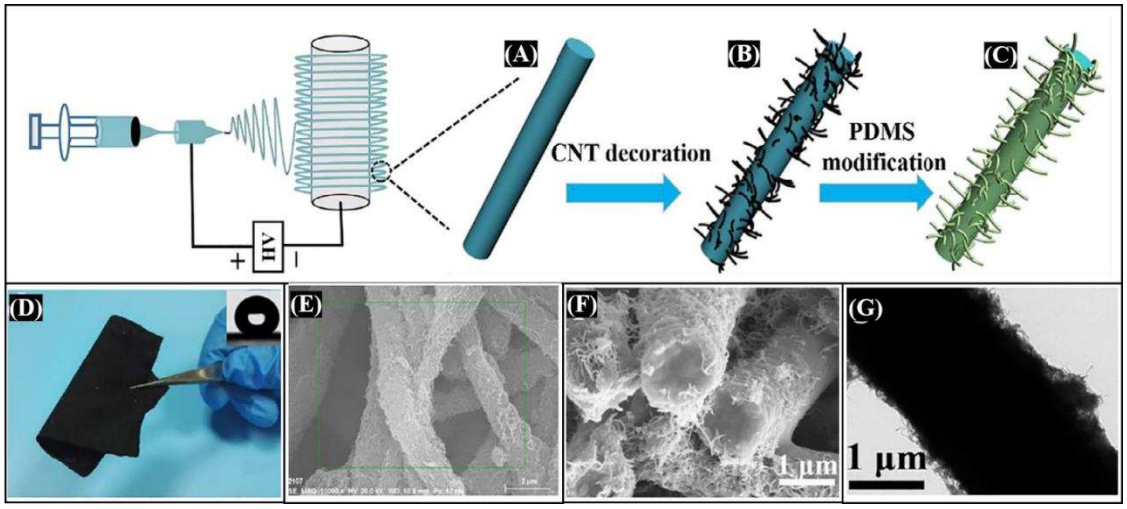

Figure 12. (A-C) Diagrammatic representation and (D) Real image, (E-G) SEM, cross-sectional SEM, and TEM view of the preparation of thermoplastic polyurethane-carbon nanotubes-PDMS based nanofiber. (Reproduced with kind permission [98]).

Table 2. Change in properties due to application of different Composite on PDMS

Type of nano-composite added	Network structure	Methods	Change in properties	Applications	Ref
MWCNT	Cylindrical fullerenes	two-step ultrasonication treatment	Leading to high stretchability, excellent electric conductivity, and electric heating performance.	Biomedical devices, wearable electronics, and strain sensors.	[99]
Silicone rubber foams (SiRFs), SiRF-GO and SiRF-GONR	Dispersible inserted layer structure	Hummers method via oxidation of natural graphite flakes	Maximum stress values at strain become 60% after assembling less contents of GONR or GO in comparison with pure SiRF materials.	Oil-water separation, sensors, biomedicine,	[100]

			The excellent flame resistance of the SiRF sample		
Polyacrylonitrile (PAN) and polyvinyl alcohol (PVA) nanofibers	Long-chain / molecular chain network	solvent mixing process and Electrospinning method	Improvements of adhesion and rheological properties. The high strength of adhesion by enhanced viscous dissipation and improved reusability	PVA/PAN core-shell nanofibers for wound dressing	[101]
TiO_2	chain network	Spin-coating method	Surfaces become hydrophobic and keep it hydrophobic even under UV light incident on it.	Oil-water separation device	[102]

3 Approaches to change in the properties of PDMS based nanocomposite

Table 2 summarizes the various nanocomposites, their network structures, change in properties, and their applications. Several properties such as mechanical, surface properties are discussed in this section.

3.1 Mechanical properties

Sun et al. performed several experiments to enhance the mechanical property of PDMS some composite with ring structure combined with PDMS. It also increases the thermal and electrical properties of PDMS. In another study, it was discovered that the MWCNT/PDMS NC can be stretched up to 280 percent, while the MWCNT NP will break at only 4% strain[1, 103–105]. PDMS film also failed at 180% elongation. But after making a compound both exhibit higher strain. To know the behavior of stress-strain curves of MWCNT/PDMS NC films in comparison to MWCNT NP and CNT[106–109]. The changes were observed on the different samples with a change in the dimension. These samples have different thickness, swelling, and CNT content[110–112]. Similarly, to find the effect of CNT content in MWCNT/PDMS, a thermogravimetric analysis was performed. Cao et al. reported the case of SiRF nanocomposite having GONR and GO sheet in a range of 0 to 0.10 wt % respectively. On the compressive test, maximum stress is 60 percent of the pure SiRF nanocomposite at a certain strain[113, 114]. If the concentration of GONR or GO increases in the composite correspondingly there are increases in maximum stress. The maximum stress of SiRF-GONR is less than that of the SiRF-GO. [115–118]. The result shows the variation of compressive stress at different concentrations of GONR and GO with pure SiRF at a different value of strain [119–121].

3.2 Thermal and Electrical Properties

Sun et al. investigated various properties of MWCNT/PDMS that are characterized as a function of applied voltage. The voltage ranges from 0 to 25 V. When voltage is applied electric current also starts increasing till the 15 V of voltage supply and obeys ohm's law[122, 123]. After 15 V voltage supply current fluctuation started and it increased nonlinearly. The temperature starts increasing after 15 V. Sun et al. investigated the change in the thermal properties. Their voltage range was from 1 to 20 V on one of the prepared samples. When applied voltage changes from 2 to 5 V, there is a small change in temperature [124, 125]. When the

constant applied voltage reaches 20 V, the temperature reached 2600 ºC within 30 s and decreases to ambient temperature when the supply voltage is stopped within 120 s. For pure SiRF 343^{0}C is the critical temperature after which it starts degrading due to thermal pyrolysis of pendant groups [126] and weight remains constant above 600 ^{0}C . It can be observed from the graph that adding a small amount of (0.10 wt%) GONR and GO increases the thermal stability of SiRF by a significant amount[127, 128]. Now the critical temperature will become 358 ^{0}C and 353 ^{0}C for SiRF-GO and SiRF-GONR respectively at 0.10% weight.

3.3 Hydrophobicity

PDMS exhibits excellent hydrophobicity which allows application in the waterproofing and coating. To enhance this property some metal oxide is used on the surface of PDMS. One of the widely used metal oxides is Titanium oxide (TiO_2). The static contact angle for water changes from 63°±1° to 103°±1°. The roughness of the TiO_2 layer is around 0.11 nm. Liu et al. [129] suggested using PDMS of thickness 2 to 4 nm and molecular weight 5 to 15 KDa to achieve hydrophobicity. The result plotted between PDMS layer thickness and molecular weight. It was plotted by taking the values of layer thickness as 0.6, 2.2, 4.0, and 5.5 nm, and corresponding molecular weights were taken as 1.3, 6.0, 17.3, and 28.0 KDa respectively. The plot obtained is a straight line having a slope of 0.66 ± 0.3. Corresponding to these values, grafting densities obtain were 2.8, 2.1, 1.3, and 1.1 × 1017/m^2. This shows that with an increase in molecular weight grafting density decreases because a polymer occupies a larger volume. Due to this, the next polymer arriving will find it difficult to form a danced layer structure[130, 131]. One of the widely used metal oxides is titanium dioxide (TiO_2). Covering its surface with PDMS to increases its hydrophobicity under UV exposure. TiO_2 was prepared from $TiCl_4$ aqueous solution when spin coated at 4000 rpm for 40 s on silicon wafer[132–135]. Keeping $TiCl_4$ at 500^0 C for 30 min to form a thin TiO_2 layer of thickness around 6 nm. On to the surface of TiO_2, trimethylsiloxy terminated PDMS was grafted,[136, 137] which was then subjected to UV light. With the help of toluene, n-hexane, and tetrahydrofuran free PDMS was washed out[138–140].

4 Applications of PDMS based nanocomposites

4.1 Gas sensing and gas separation using PDMS

Gas separation systems based on membranes may save a lot of energy compared to traditional separation methods. The permeability and selectivity of polymeric membranes are typically limited by a trade-off: as selectivity rises, permeability falls, and vice versa[141, 142]. To determine the applicability of PDMS for Freon/permanent gas separations, Roberts et al. [143] measured the permeability of PDMS-based composite membranes to different Freon and carbon tetrafluoride. They discovered that nitrogen was more permeable than carbon tetrafluoride in PDMS. When compared to the pristine PDMS membrane, the gas permeability of Ar, CO_2, CH_4, and N_2 was improved as a result of fabricating the membrane based on PDMS/graphene nanocomposite. This is accomplished by producing interfacial gaps between graphene flakes and polymer chains, which increases the nanocomposite's free volume fraction and therefore its permeability[144]. In PDMS, 0.25 wt % graphene loading is optimal, however higher graphene loading might cause create aggregation and hence limit the surface characteristics. The solution-diffusion mechanism controls gas permeation through a rubberized polymer. Adsorption at the upstream border, diffusion through the membrane, and desorption at the downstream boundary are the three processes in this mechanism. The change in gas molecule diffusion across the composite material causes an increase in penetration for all gases(see figure 13(A-C)). The presence of graphene in the PDMS matrix has the capacity to form

permanent gaps at these interfaces, enabling diffusion. As a result of the addition of graphene to the PDMS matrix, the amount of free volume within the polymer increases, resulting in increased permeation. Figure 13D compares the performance of graphene membranes to PDMS and no membrane. As can be observed, the sensor response of the graphene-PDMS nanocomposite membrane is nearly identical to that of a membrane that isn't there at all. When compared to the PDMS reference membrane, however, the composite material performs significantly better, with less attenuation and a far faster reaction. This implies that the membranes are practically transparent to gas molecules and can provide excellent solutions for monitoring gases while keeping the sensor separated from pollutants in the environment. The hydrophobic findings of produced membranes and response towards CO_2 gas are shown in figure13(E-F)).

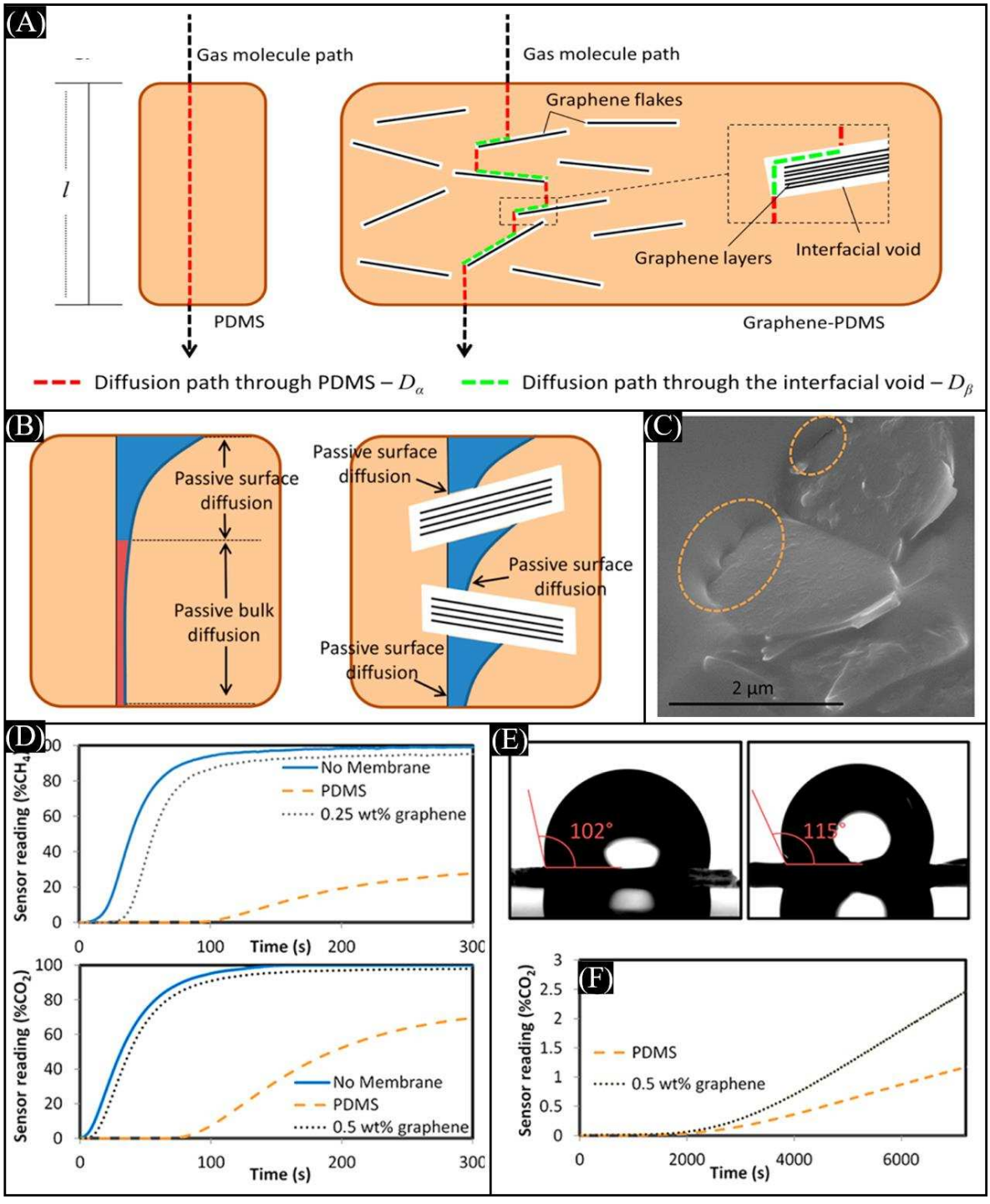

Figure 13. (A)Schematic of the diffusion paths, (B) the bulk and passive surface diffusion of gas molecules of pure PDMS and graphene-embedded PDMS nanocomposites, and (C) SEM images of 0.25 wt% graphene-doped PDMS nanocomposites showing the formation of nano–to– meso-sized voids around the flakes and that the polymer does not efficiently make strong bonds with the surface of the flakes. (D) Response of CO_2 and CH_4 permeation, (E) contact angle, and (F) response to CO_2 of pure PDMS and 0.5 wt% graphene-embedded PDMS. (Reproduced with kind permission [144]).

In another research, PDMS composites with various weight quantities of multi-walled carbon nanotubes (MWCNT) were synthesized as membranes in order to test gas separation capabilities. To facilitate effective and uniform dispersion of MWCNT within the PDMS, MWCNTs were first dispersed in toluene and added in PDMS. The mixture is then placed in a magnetic stirrer and at 75 ˚C for 60 min to evaporate toluene. The curing agent is then added to the prepared mixture in a 1:1 weight ratio to the PDMS elastomer, and the mixture is mixed for 15 minutes before being placed in a petri dish, degassed, and cured at room temperature to obtain MWCNT/PDMS membrane. The membranes' selectivity for separating hydrogen from carbon tetrafluoride gas was tested. Membranes containing 1% MWCNT enhanced hydrogen gas selectivity by 94.8 percent. Furthermore, at MWCNT concentrations larger than 5%, carbon tetrafluoride permeability across membranes was virtually completely prevented. Figure 14 shows (A) gas sensing setup, (B) SEM images of 5wt% and 10wt% MWCNT/PDMS nanocomposite, and (C) sensor resistance vs time relationship[145],[146].

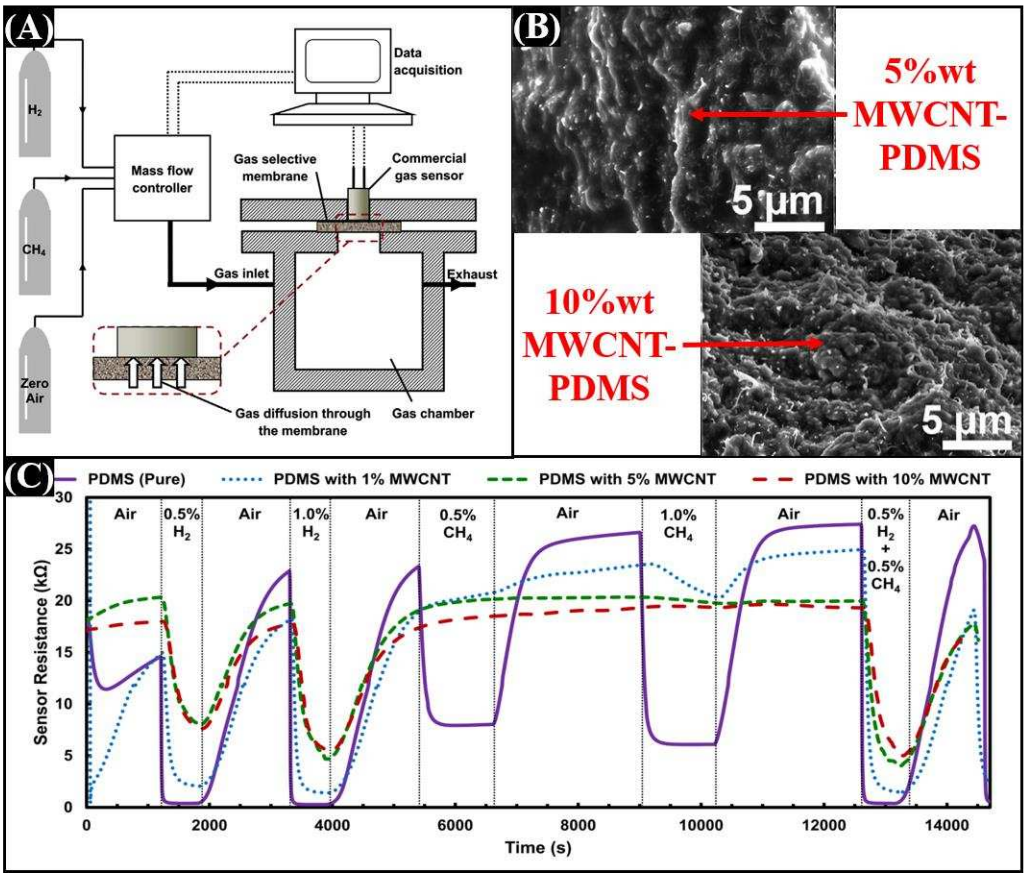

Figure 14. (A) Diagrammatic representation of gas sensing instrument with sensing film, (b) SEM images of 5wt% and 10wt% MWCNT/PDMS nanocomposite membranes, (c) membrane resistance response towards H_2 and CH_4 gas. (Reproduced with kind permission[145])**.**

In another research, Firpo et al. [147] investigate the He and CO_2 permeability of PDMS membranes with thicknesses less than 55 microns using a high vacuum setup with a quadrupole mass spectrometer. A thick PDMS layer is supported by a glass coverslip. A 10:1 PDMS elastomer and its curing agent are combined and placed in a vacuum desiccator for 20 minutes to eliminate any bubbles before spinning for 1 minute on a glass coverslip and heating for 60 minutes at 100 °C. The layer is then treated with an oxygen plasma for

1 min before being silanized in a vacuum chamber for 30 minutes using an anti-stiction agent. The PDMS membrane is then spin-coated on the anti-stiction layer and baked at 70˚C. The PDMS membrane is now gently squeezed with tweezers and baked for 15 minutes at 60°C. Finally, the PDMS membrane is placed on the previously prepared support. For thicknesses lower than a few micrometers, the analysis reveals a thickness-dependent permeability. Hwang et al.[148] introduce a robust and cost-effective approach for uniform deposition of oxide Nanowires across a specific electrode region by coating with a solution containing Nanowires following PDMS patterning. The hydrophobic PDMS guiding barrier prevented the deposited solution from extending out, allowing the density of the Nanowires in the sensor to be easily adjusted. The high-density NW sensor enhanced NO_2, CO, C_2H_5OH, and C_3H_8 sensitivity while reducing the speed of gas recovery and response. With the help of Sn metal, tin oxide nanowires are developed in the gas phase. On the Al_2O_3 boat, the source is loaded. An Au-coated Si wafer was put 5 cm downstream from the source and reacted for 20 minutes in a horizontal furnace with the source and 0.5 sccm of O_2 gas to create a nanowire. Using a DC sputtering approach, a layer of Ti and Pt with thicknesses of 50 and 300 nm is deposited on a silicon dioxide/silicon wafer, and comb-like electrodes are created using a lift-off procedure(see figure 15 (A)). The PDMS elastomer and curing agent were then mixed 9:1 and poured on top of the substrate, which was then cured for 5 hours at 60°C. Above the electrode region, square holes are cut to generate PDMS patterning, which is then removed using tweezers (see figure 15(B)). Ultrasonication was used to disperse the as-grown 0.01 g tin oxide Nanowires in a solution containing 10 ml of DI water and propanol-2. Using a micro-pipette, a slurry droplet comprising tin oxide nanowires was deposited onto the PDMS patterned substrate and dried gradually (see figure 15(C-E)). , Very-low density, Low-density, and high-density nanowires sensors were made by varying the number of droplets of the slurry, respectively. At 400˚C, the gas sensing properties of 100 ppm C_3H_8, CO, and C_2H_5OH are measured. The gas response was found to be (a)1.6, 1.81, and 3.3, (b) 1,8, 1,6, and 23.8, (c) 2.98, 3.95, and 42.6, for very low density, low density, and high density respectively. By increasing the density of the nanowires, the gas sensitivity was enhanced by approximately 13 times, but the response rate and recovery rate dropped.

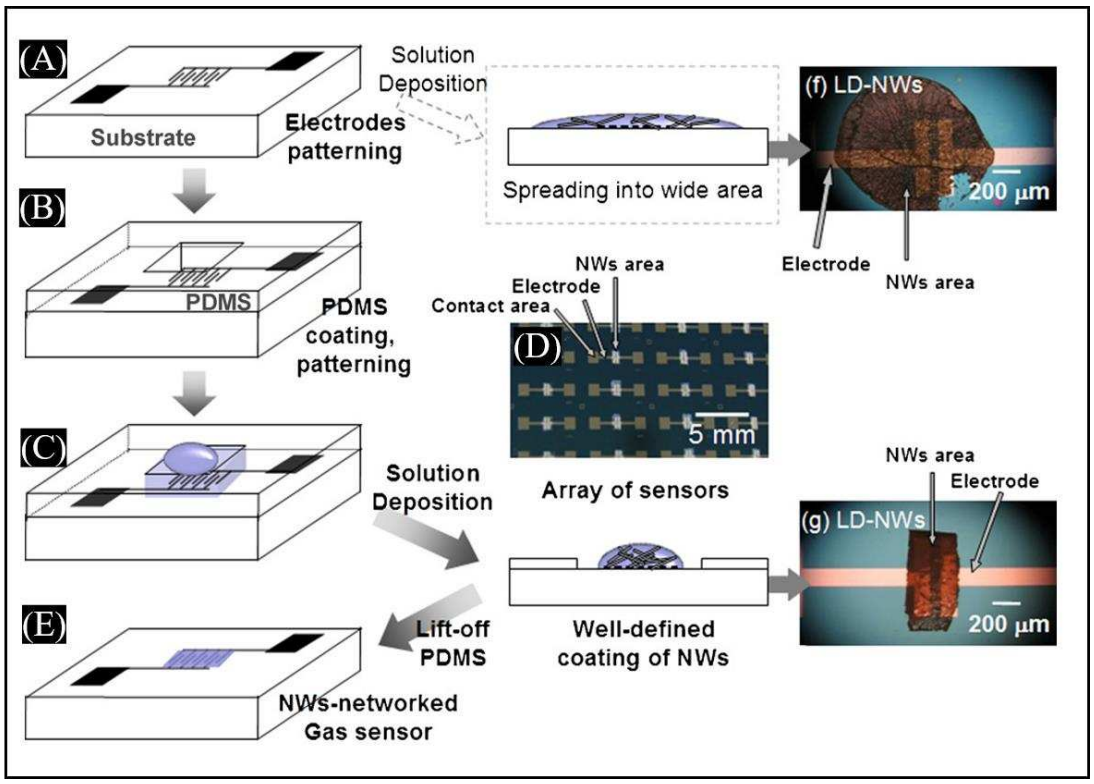

Figure 15. Schematic representation of fabrication step for the nanowire networked-based gas sensor. (Reproduced with kind permission [148]).

According to Gao et al. [149], covering a gas sensor with a hydrophobic PDMS layer enhances moisture resistance substantially. An ambient temperature gas sensor, titanium oxide nanotubes(NTs) coated with Pd were used. A simple thermal evaporation procedure may be used to apply the conformal PDMS layer to nanostructured sensor materials. The PDMS layer not only offers a hydrophobic surface for water droplets on the sensor, but it is also thick enough to effectively prevent water molecules from penetrating. Other hydrophobic alteration layers, on the other hand, can only turn a gas sensor into superhydrophobic but not humidity resistant. Furthermore, by protecting palladium nanoparticles on the gas sensors surface, the PDMS layer increases the long-term stability of Pd-doped TiO_2 nanotube sensors. Figure 16(A) shows the preparing steps for PD-doped TiO_2 nanotubes. The pure Pd-doped TiO_2 nanotubes were firstly placed in a closed container with a newly prepared PDMS stamp to synthesis PDMS-Pd-doped TiO_2 nanotubes. The container was placed in the oven for 20 minutes at 235°C before being made to cool naturally. As a result, Volatile silicone molecules in the form of short PDMS chains create a conformal layer on the surface of the Pd-doped TiO_2 nanotube and then crosslink. It works as a moisture barrier and acts as a passivation layer. Figure 16(B) indicates that when Pd-doped TiO_2 nanotube is coated with PDMS, there is no discernible variation in morphology, and both Pd-nanoparticles and titanium oxide nanotubes are stable during the PDMS deposition process. Figure 16(C-D) shows the sensing response of pure Pd / TiO_2-nanotube, which declines with rising RH, with only around 10% response value remaining at 75% RH compared to 25% RH. PDMS-Pd-doped TiO_2 nanotube, on the other hand, exhibits complete moisture resistance under optimal circumstances. The thickness of the PDMS layer plays a significant influence, according to the results of the experiments.

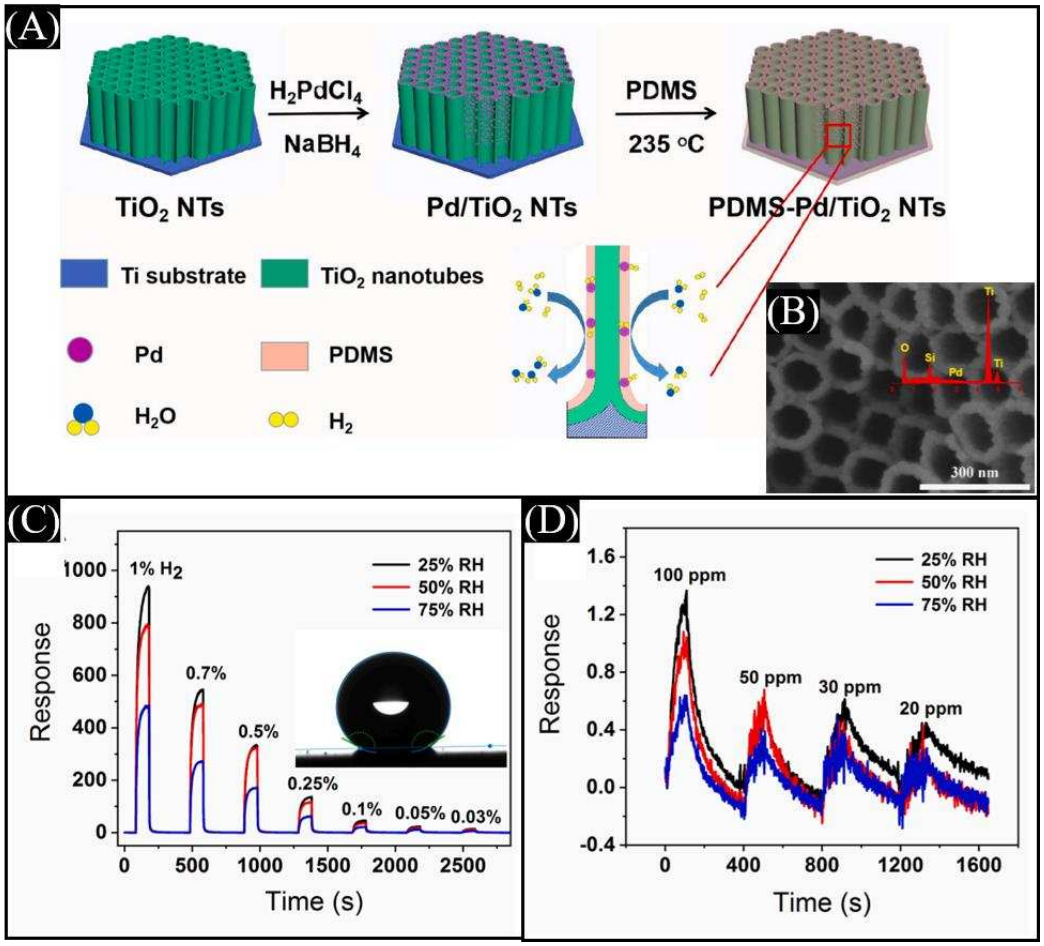

Figure 16. (A) Diagrammatic representation, (B) SEM views with EDS results, and (C-D) Real-time monitoring of the fabricated PDMS coated Pd-doped titanium oxide nanotubes. (Reproduced with kind permission[149]).

He [150] has invented a novel energy-independent active gas sensor for real-time automobile emissions monitoring. A (PDMS-polypyrrole (ppy) triboelectric gas detecting unit array was used to make the tubular device. Because the output current signal is dependent on the type and concentration of the target gas (such as NO, NH_3, CO) in the gas flow, it may be utilized as a measuring signal. Seven gas sensors based on different derivatives of ppy are built to detect various gases. The coupling effect of PDMS/ppy and the gas-sensing characteristics of ppy is thought to constitute the operating mechanism. The device may be put in an automobile's tailpipe, it can now analyze exhaust gas in real-time without the use of additional equipment(see figure 17(A)). The preparation of a gas sensor begins with the photolithographic process, in which patterns are produced on Cu foil. The copper foil was washed many times with ethanol and DI water. Following that, a spin coating of 3ml of positive photoresist for 15sec, and 40sec at 200 and 1500 rpm was performed. The copper foil was then heated for 150 sec at 100°C, followed by a photolithography step to result in the desired pattern. The prepared copper foil was then submerged in the developer for 1 min before being rinsed with DI water. Etching was then used to remove the patterned copper array. The PDMS elastomer and curing agent are then combined and poured onto the copper array design for spin coating, followed by curing at 90 C for 0.5 hours. The copper array design was then etched again to provide enough gap between the copper array and PDMS for friction and to allow for the deposition of Ppy. The PDMS

film's surface was then dry-etched using an inductively coupled plasma method. Seven derivatives of ppy were then electrochemically polymerized onto the copper circuit, resulting in seven independent gas measuring units(see figure17 (B)). Figure 17(D-G) shows the SEM images and figure 17(H) shows the working principle of the gas sensor.

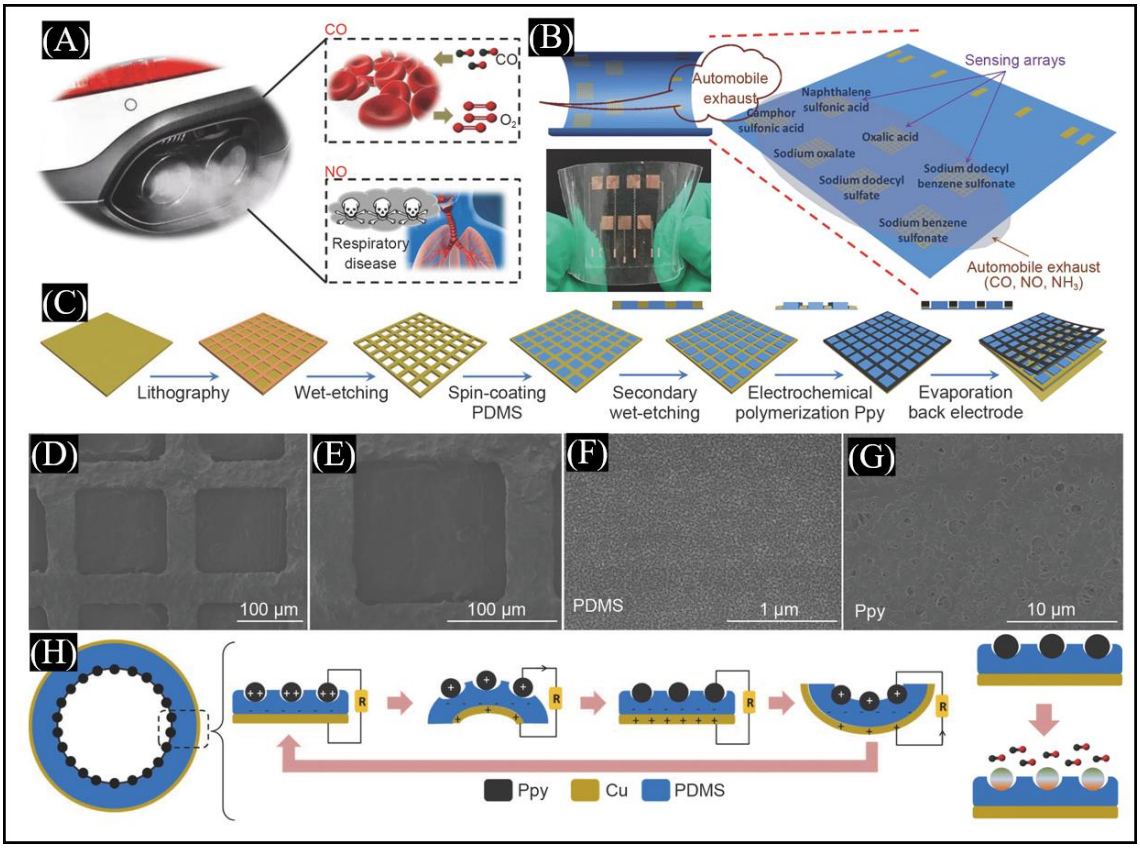

Figure 17. (A) The effects of automobile exhaust gas on the human body, (B) Gas sensor design for exhaust gas analysis. (C) Fabrication of gas sensor. SEM images of (D, E) a single gas-sensing unit, (F) PDMS, and (G) Ppy–NSA. (H) Working mechanism. (Reproduced with kind permission [150]).

Zhou et al. [151] used the array of ZnO-ZIF71-PDMS NRs to create a gas sensor with high sensitivity and selectivity for detecting acetone. By using the vapor deposition technique, PDMS was deposited on ZnO @ ZIF71 surface. The novel sensor exhibits an efficient response towards acetone and ethanol. The PDMS membrane functions as a chemical filter, exhibiting acetone selectivity and eliminating the ethanol response at a low level of concentration. CVD technique is used to produce ZnO-ZIF71-PDMS nanorods. The PDMS membrane has an adverse influence on ethanol gas sensing ability. In contrast, ZnO-ZIF-71-PDMS nanorods had only a minor inhibitory impact on the response towards acetone. The working mechanisms of the prepared gas sensor are shown in figure 18A. Before reaching the ZnO-ZIF71 surface, ethanol and acetone should penetrate through the prepared PDMS, this can be explained by the solution diffusion model. It is divided into three processes, (a) sorption, (b) diffusion, and (c) desorption. Because the desorption process is substantially quicker than the prior two processes, sorption and diffusion are the rate-determining phases. With the coating of PDMS, the contact angle of ZnO-ZIF71 nanorod changes from 112˚ to 139˚(see figure 18C). The two gas sensors were subjected to ethanol/ acetone to evaluate their gas detecting capabilities (see figure 18B).

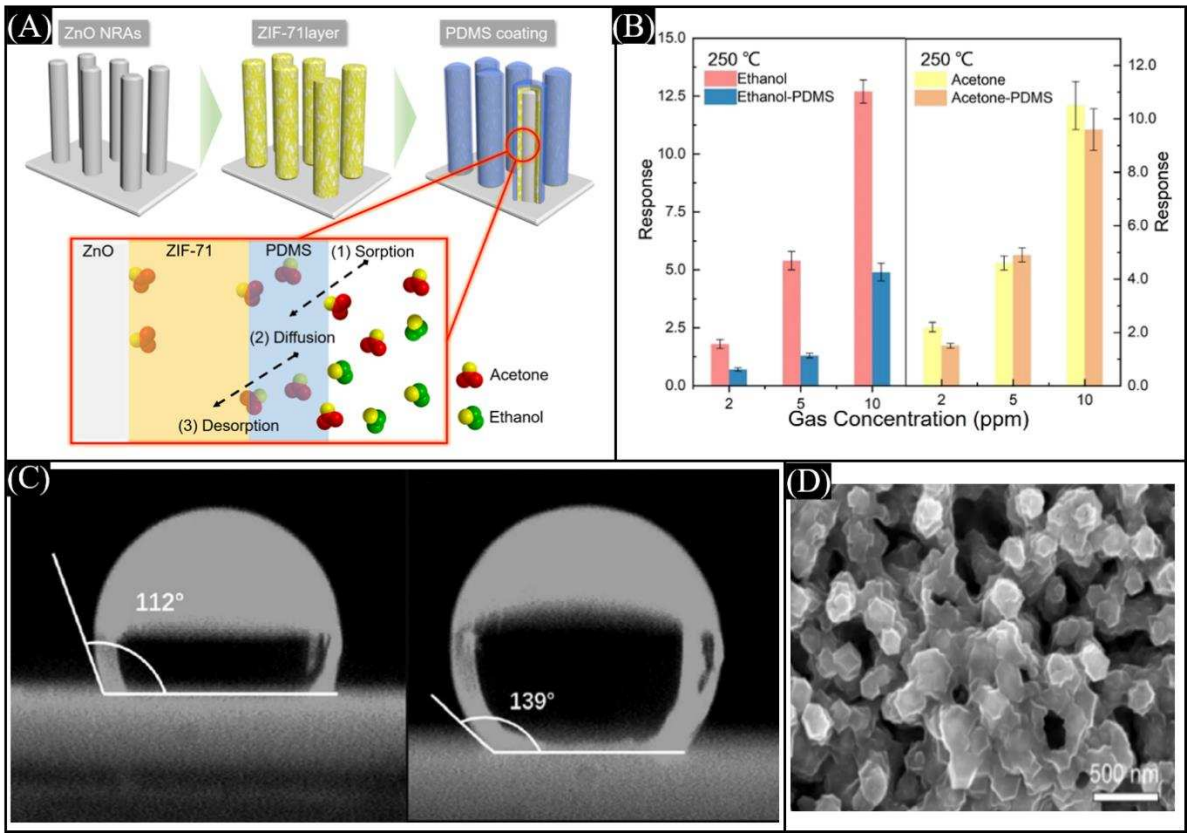

Figure 18. (A) Diagrammatic representation of ZnO-ZIF71-PDMS nanorods and their working mechanisms, (B) Gas sensing response of ZnO-ZIF71 and ZnO-ZIF71-PDMS samples to acetone and ethanol at 250°C. (C) Contact angle of ZnO-ZIF71(CA: 112), and ZnO-ZIF71-PDMS(CA;139), (D) SEM image of ZnO-ZIF71-PDMS. (Reproduced with kind permission [151]).

Nam et al. [152] developed an easy-to-follow approach for making spiropyran-PDMS films. In the PDMS film, the photochemically produced ring-opened ME form(spiropyran) is quickly protonated by hydrochloric gas to yield the nonfluorescent MEH form(spiropyran). Images of spiropyran- PDMS film before and after UV irradiation for 180 sec at 365 nm are shown in Figure 19. When the material is exposed to UV light, it becomes purple, indicating the formation of (ME form)spiropyran in the produced membrane. When the material is irritated by visible light, the process changes (shows decoloration). We observed that HCl vapor may permeate the PDMS layer while examining hydrochloric vapor-induced chromium transfer of PDMS film embedded in spiropyran. As a result, extended exposure to hydrochloric vapor on a PDMS film containing ME-type (spiropyran) causes the color to shift from purple to yellow, even on the backside of the membrane, which is not in direct interaction with the gas. This result implies that Hydrochloric gas molecules diffuse through the PDMS coating, converting ME to the MEH form of spiropyran.

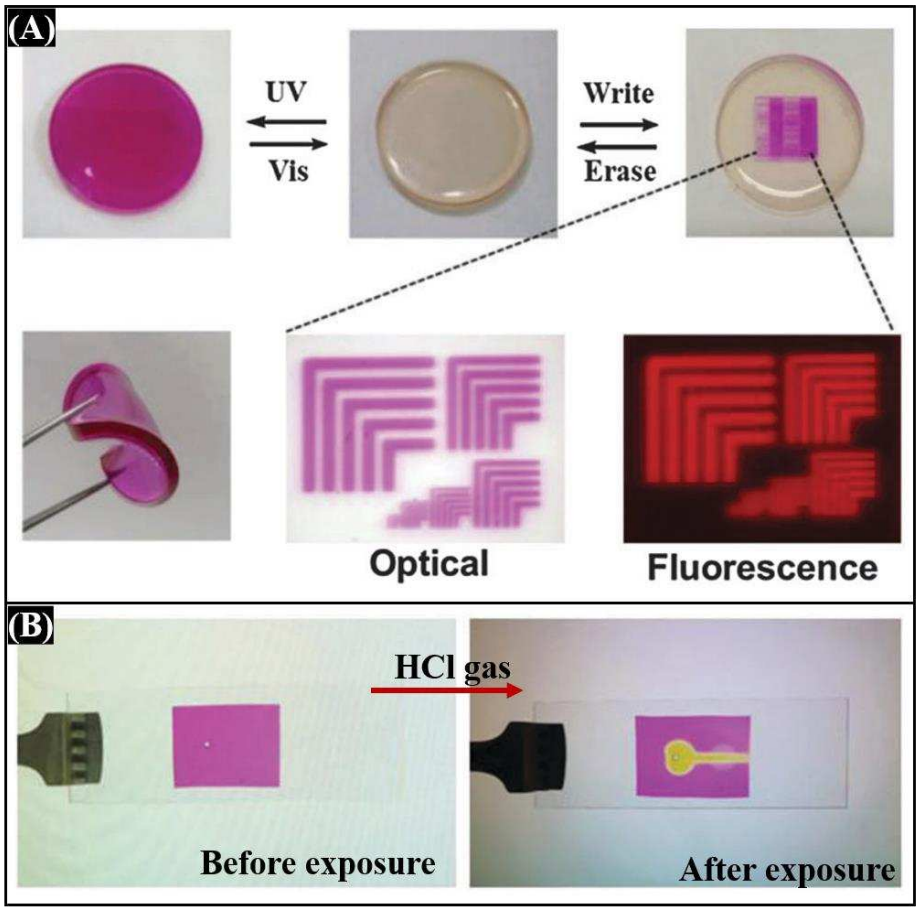

Figure 19. (A) A spyropyran–embedded PDMS hybrid film was produced (center), after 180 sec of UV exposure (left), and patterned images were obtained by photo-masked UV exposure (right). With zoomed microscopic images of a UV-exposed flexible membrane, optical, and fluorescence of the patterned film, and (B) images of a spyropyran–embedded PDMS before (left) and after (right) HCl gas exposure. (Reproduced with kind permission [152]).

4.2 Others sensing applications of PDMS

4.2.1 Flexible strain sensor

Flexible ultrasensitive piezoresistive strain sensors were fabricated by CO_2 Laser ablating of the surface of the multiwall carbon nanotube/polydimethylsiloxane (MWCNT/PDMS) composite film prepared by a coating process[153–156]. After laser ablating, MWCNT/PDMS film was greatly improved in its electrical conductivity and sensing gauge factor, by adding only 1.0 wt% of MWCNT[157–160]. Chowdhury et al. fabricate a flexible and stretchable nanocomposite based on PDMS/CNF for the application of piezoresistive sensing function. The uniform dispersion of CNF-PDMS has produced a repeatable sensing response of ~30% tensile strain and shows an electric conductivity of 10^2 S m^{-1}. The author reported the testing of compressive strain for cylinder and truncated cone shape with having a gauge factor of 18.3 and 6.3 respectively. Hassan et al. proposed a flexible strain sensor based on the Ge/ZnO nanocomposite layer fabricated on the random ridge type thick PDMS material which finds its application in the field of wearable electronics due to their improved stretchability and flexibility response. The results reveal stretchability up to ~30% and flexibility up to 10 mm bending diameter [161]. Luo et al. fabricated a polymer film by

blending PEDOT: PSS into the PDMS matrix. The doping with the mixture of 7wt% EG and 10wt% Triton X-100 into the conductive polymer shows lowest sheet resistance value of 20 Ωsq^{-1} [162]. Rajtha et al. fabricated a transparent nanocomposite with combining low volume percentage chemically treated r-GO filler into the PDMS. Due the accumulation of the r-GO fillers into the PDMS matrix, the mechanical deformation of the nanocomposite's experiences bending, twisting, and stretching and therefore becomes rigid and less elastic. The result shows that with the introduction of only 0.018 volume % r-GO filler exhibits increased the optical transparency up to 82% and 16 times higher dielectric constant in contrast to PDMS [163]. Shi et al. prepared a PDMS sub-microbeads/GO nanocomposite ink having a thixotropic and viscoelasticity properties for the direct ink writing (DIW). The slight thermal annealing on the DIW printed devices shows a low sheet resistivity value of 1660 Ω-cm, at a percolation threshold of 0.83 volume% GO. These nanocomposites find its application in the field of strain sensing and pressure sensing as the obtained pressure sensitivity is 0.31 kPa^{-1} at operating pressure range of 0.248-500 kPa [164].

4.2.2 Blood-Brain Barrier Research

Blood-brain barrier[165] is the semipermeable membrane of endothelial cells[166] that blocks toxicants that prevents drug penetration for the central neural system[167]. Lab on the chip is a tool used to understand the dynamic behavior of blood-brain barrier[167, 168]. This can be achieved by two methods, the first is the PDMS chamber is incorporated with polycaprolactone coated sugar microfibers which will further dissolve to get a microtube and the second is an Electrospinning core-sheath and incorporated in a bridge between two PDMS reservoirs[169–171].

4.2.3 Flexible and wearable electronics

Esfahani et al. has fabricated and measured the properties of the MWCNTs/PDMS nanocomposites in AC and quasi-AC electric field. The properties of a homogeneous and non-agglomerated MWCNTs/PDMS nanocomposite are influenced by the concentration of the CNT, which can be achieved at a voltage of 1075V zero to peak at a frequency of 100 Hz with 35 milliamps current at 80 ˚C. The creation of penetrating networks by CNT in PDMS results in an increase in electrical conductivity from 30000 10^{-11} S/cm to 100000 10^{-11} S/cm [172]. Attila et al. fabricated and tested the surface-enhanced Raman spectroscopy (SERS) with the gold (Au)/silver (Ag)-PDMS nanocomposite layer using a method of reduction of chloroauric acid or silver nitrate solution by PDMS [173]. Wu et al.[174] verified the possibility of CNT/PDMS-based nanocomposite films to be used as flexible electronics due to their ease of micromachining and even electrical properties. The CNT/PDMS film with various thicknesses is fabricated and checked for the dependency of the rapid drop of the conductivity. Promsawat et al. developed and characterized flexible piezoelectric nanoparticle composites based on lead magnesium niobate titanate (PMNT) nanoparticles in a PDMS polymer matrix using the columbite precursor technique. The spin coating method is used for the preparation of the PMNT/PDMS nanocomposites follow by the addition of the CNTs in order to improve the cross-linking of PMNT nanoparticles with the PDMS polymer matrix. Under a load condition of 300 N, the fabricated nanocomposite with a surface area of ~300 mm^2 can generate an open circuit voltage of 2.83±0.24 V and a short circuit current of 0.33±0.01 μA [175]. Jang et al. demonstrated the use of a PEDOT/PSS thin layer coated on biomimetic polydimethylsiloxane substrate to fabricate a flexible piezoresistive pulse sensor (FPPS). The sensitives of the device were 62.56 kPa^{-1} and 8.32 kPa^{-1} in low pressure and high pressure ranges respectively [176]. Gao et al. fabricated a pressure sensor based on a flexible PDMS/CNT microsphere and compares the outcomes with the flat configuration. The results show

the improved sensitivity of -0.111 kPa^{-1} with a low detectable pressure of 0.02 kPa, these sensors find their application to measure real-time pulses signal, muscle activity, and various applications in monitoring the human physiological parameters [177].

4.2.4 Removal of chemical hazards from wastewater

Majooni et al. investigate the removal of styrene from wastewater via fabricating the nanocomposite composed of PDMS and reduced graphene oxide (rGo) fillers. The presence of the graphene oxide in the PDMS matrix controls the enlargement of the prepared film and improves its solubility parameter and thermal stability towards styrene. The pervaporative parameter of the fabricated film shows the separating factor of the optimum film was increased about 250%[178]. Saharudin et al. reported a simple spraying methodology for creation of a PDMS/Ge super-hydrophobic coating layer on a glass surface. To investigate the superhydrophobic behavior of the fabricated film, the author mixes three different types of graphene with PDMS. The fabricated film is dried at 80 ˚C and to measure the wettability of the surface, parameters such as water contact angle and sliding angles were investigated. The results display that the graphene (G)-PDMS coating shows better stabilities in contrast to graphene oxide (GO)-PDMS and modified graphene oxide(mGO)-PDMS matrix[179]. Bae et al. introduce oligosaccharides in the fabricated PDMS/Ge nanocomposites for the detection of the chemical hazards present in the environment. On increasing the concentration of 1.2 wt% Ge the electrical conductivity of the PDMS/Ge nanocomposites shows momentous variations. The output of this sensor system is evaluated using different concentrations of a model analyte, methylparaben, and it yielded a detection limit of ~10 nM [180]. Basu et al. report the use of various GO/PDMS nanocomposite concentrations to boost the dynamic actuation and electrowetting of a conductive droplet over a dielectric substrate [181]. The composite's dielectric constant is enhanced by adding the w/w% of GO in the PDMS matrix to ~2.65 %w/w until the percolation limit is met.

4.2.5 Pressure sensor

In a Pressure conductive rubber sensor, liquid-metal-polydimethylsiloxane is used for fabrication. It is a composite of Galinstan and PDMS. The mechanical strength and electrical credibility of composite make its application suitable for the human body. Initially, the composite is not conductive but after applying pressure or strain more than the threshold value it becomes conductive. The applying threshold value depends upon the ratio of Galinstan and PDMS. It can be used to measure blood pressure and respiration rate. The variation of the applied threshold value at different ratios of the composite can be seen in the work done by Jun Ho Oh[182, 183]. Memon et al. fabricate a piezoresistive-based pressure sensor with a combination of soft mixing of polydimethylsiloxane and a hybrid Carbon black (CB) and CNT for the application in observing respiratory disorders. The fabricated device shows a change in resistance to be greater than 0.4% under the application of 37Pa pressure[184]. Zhai et al. fabricate a porous foam pressure sensor using a combination of carbon black CB/PDMS nanocomposite via ultra-sonification technique. The sensor shows a high linear working range up to 91% with excellent response stability and time of 45ms. With superior durability of greater than 15000 cycles. This nanocomposite form exhibits a great ability to detect human activities such as walking, jumping, bending of fingers and elbows as well as having an excellent ability of oil/water separation [185]. A facile circuit is assembled by using our conductive CB/PDMS foam to observe the compression sensing performance, as shown in figure 20a. Interestingly, the brightness of the lamp changes in the process of compressing and releasing the CB/PDMS foam. More

concretely, the LED lamp becomes bright when the CB/PDMS foam is compressed and becomes dark again when it is released(see figure 20(b-c)).

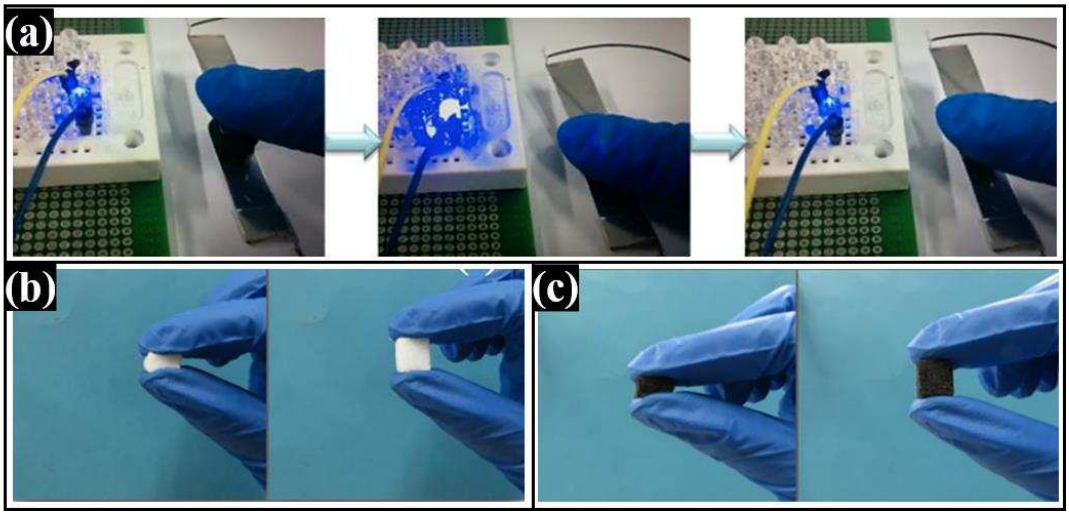

Figure 20. (A) A circuit made out of carbon black/PDMS foam. The variation of brightness of LED varies with the compression and release of (B) the pure PDMS (white) and (C) carbon black/PDMS (black) foams. (Reproduced with kind permission [185]).

5 Conclusions

The review work summarizes the various fabrication approaches, change in the properties of the PDMS on combining it with different nanocomposites and metal oxides. This provides the relation between microstructure and functional properties of PDMS. By improvising the properties of PDMS, its utility can be further extended to the domain of soft robotics, aerospace, medical assistance, etc. Despite the various advancements in this field, there are still a few challenges on which work is needed to be performed in near future. The very first one is the scalability of the PDMS composites manufacturing. Although PDMS is convenient in processability the high price limits the use of PDMS in large volume manufacturing. The other challenge is to bring the persistency of the PDMS surface i.e. how long the surface of the PDMS will be hydrophobic is the challenge. To prevent this, proper design and introduction of the correct function group in the polymer will be the step towards future work. This review work will certainly assist in better understanding and improving the knowledge of PDMS nanocomposites to overcome the challenges for future researches.

Acknowledgment

The corresponding author wishes to acknowledge the Startup Research Grant (SRG/2020/001895) provided by Science and Engineering Research Board, Department of Science and Technology, India.

Statements and Declarations

Authors declare that there is no conflict among the contributing authors related to the financial or non-financial interests that are directly or indirectly related to the work submitted for publication.

References

[1] Sengupta, R.; Chakraborty, S.; Bandyopadhyay, S.; Dasgupta, S.; Mukhopadhyay, R.; Auddy, K.; Deuri, A. S. A Short Review on Rubber/Clay Nanocomposites with Emphasis on Mechanical Properties. *Polym. Eng. Sci.*, **2007**. https://doi.org/10.1002/pen.20921.

[2] Paul, D. R.; Robeson, L. M. Polymer Nanotechnology: Nanocomposites. *Polymer*. 2008. https://doi.org/10.1016/j.polymer.2008.04.017.

[3] Potts, J. R.; Dreyer, D. R.; Bielawski, C. W.; Ruoff, R. S. Graphene-Based Polymer Nanocomposites. *Polymer*. 2011. https://doi.org/10.1016/j.polymer.2010.11.042.

[4] Verma, G.; Mondal, K.; Gupta, A. Si-Based MEMS Resonant Sensor : A Review from Microfabrication Perspective. *Microelectronics J.*, **2021**, *118*, 1–64. https://doi.org/10.1016/j.mejo.2021.105210.

[5] Kishnani, V.; Verma, G.; Pippara, R. K.; Yadav, A.; Chauhan, P. S.; Gupta, A. Highly Sensitive, Ambient Temperature CO Sensor Using Tin Oxide Based Composites. *Sensors Actuators A Phys.*, **2021**, *332*, 113111. https://doi.org/10.1016/J.SNA.2021.113111.

[6] Chauhan, P. S.; Rai, A.; Gupta, A.; Bhattacharya, S. Enhanced Photocatalytic Performance of Vertically Grown ZnO Nanorods Decorated with Metals (Al, Ag, Au, and Au–Pd) for Degradation of Industrial Dye. *Mater. Res. Express*, **2017**, *4* (5), 055004. https://doi.org/10.1088/2053-1591/AA6D31.

[7] Biswal, H. J.; Vundavilli, P. R.; Gupta, A. High Aspect ZnO Nanorod Growth over Electrodeposited Tubes for Photocatalytic Degradation of EtBr Dye. *RSC Adv.*, **2021**, *11* (3), 1623–1634. https://doi.org/10.1039/d0ra08124h.

[8] Gupta, A.; Pandey, S. S.; Bhattacharya, S. High Aspect ZnO Nanostructures Based Hydrogen Sensing. *AIP Conf. Proc.*, **2013**, *1536* (2013), 291–292. https://doi.org/10.1063/1.4810215.

[9] Singh, P.; Kant, R.; Rai, A.; Gupta, A.; Bhattacharya, S. Materials Science in Semiconductor Processing Facile Synthesis of ZnO / GO Nano Fl Owers over Si Substrate for Improved Photocatalytic Decolorization of MB Dye and Industrial Wastewater under Solar Irradiation. *Mater. Sci. Semicond. Process.*, **2019**, *89*, 6–17. https://doi.org/10.1016/j.mssp.2018.08.022.

[10] Sheshkar, N.; Verma, G.; Pandey, C.; Kumar, A.; Ankur, S. Enhanced Thermal and Mechanical Properties of Hydrophobic Graphite - Embedded Polydimethylsiloxane Composite. *J. Polym. Res.*, **2021**, *28* (403), 1–11. https://doi.org/10.1007/s10965-021-02774-w.

[11] Kumar Verma, G.; Ansari, M. Z. Design and Simulation of Piezoresistive Polymer Accelerometer. *IOP Conf. Ser. Mater. Sci. Eng.*, **2019**, *561* (1). https://doi.org/10.1088/1757-899X/561/1/012128.

[12] Gupta, A.; Pal, P. Flexible Sensors for Biomedical Application. *Energy, Environ. Sustain.*, **2018**, 287–314. https://doi.org/10.1007/978-981-10-7751-7_13.

[13] Sharma, A. K.; Sheshkar, N.; Gupta, A. Static and Dynamic Stability of Dielectric Elastomer Fiber Composites. *Mater. Today Proc.*, **2021**, *44*, 2043–2047. https://doi.org/10.1016/J.MATPR.2020.12.151.

[14] Atwe, A.; Gupta, A.; Kant, R.; Das, M.; Sharma, I.; Bhattacharya, S. A Novel Microfluidic Switch for PH Control Using Chitosan Based Hydrogels. *Microsyst. Technol.*, **2014**. https://doi.org/10.1007/s00542-014-2112-0.

[15] Singh, R. K.; Kumar, A.; Kant, R.; Gupta, A.; Suresh, E.; Bhattacharya, S. Design and Fabrication of 3-Dimensional Helical Structures in Polydimethylsiloxane for Flow Control Applications. *Microsyst. Technol.*, **2014**, *20* (1), 101–111. https://doi.org/10.1007/s00542-013-1738-7.

[16] Chen, G.; Svec, F.; Knapp, D. R. Light-Actuated High Pressure-Resisting Microvalve for on-Chip Flow Control Based on Thermo-Responsive Nanostructured Polymer. *Lab Chip*, **2008**, *8* (7), 1198–1204. https://doi.org/10.1039/b803293a.

[17] Reyes, D. R.; Iossifidis, D.; Auroux, P.; Manz, A. Micro Total Analysis Systems . 1 . Introduction , Theory , and Technology. **2002**, *74* (12), 2623–2636.

[18] Kishnani, V.; Park, S.; Nakate, U. T.; Mondal, K.; Gupta, A. Nano-Functionalized Paper-Based IoT Enabled Devices for Point-of-Care Testing: A Review. *Biomed. Microdevices*, **2022**, *24* (1). https://doi.org/10.1007/S10544-021-00588-7.

[19] Gupta, A.; Patel, V. K.; Pandey, C. Functional Characterization of Nano-Porous Silicate-Polymer Composite for Bovine Serum Albumin Immobilization. *Sensors Int.*, **2021**, *2*, 100080. https://doi.org/10.1016/J.SINTL.2021.100080.

[20] Biswal, H. J.; Rout, P.; Vundavilli, P. R.; Gupta, A. Laser-Assisted Microhole Fabrication in a Flexible Polymer Substrate. *Lasers Eng.*, **2021**, *49* (1), 3–20.

[21] Gupta, A.; Sundriyal, P.; Basu, A.; Manoharan, K.; Kant, R.; Bhattacharya, S. Nano-Finishing of MEMS-Based Platforms for Optimum Optical Sensing: *J. Micromanufacturing*, **2019**, *3* (1), 39–53. https://doi.org/10.1177/2516598419862676.

[22] Nguyen, N. T.; Huang, X.; Chuan, T. K. MEMS-Micropumps: A Review. *Journal of Fluids Engineering, Transactions of the ASME*. 2002. https://doi.org/10.1115/1.1459075.

[23] Jeon, N. L.; Chiu, D. T.; Wargo, C. J.; Wu, H.; Choi, I. S.; Anderson, J. R.; Whitesides, G. M. Design and Fabrication of Integrated Passive Valves and Pumps for Flexible Polymer 3-Dimensional Microfluidic Systems. *Biomed. Microdevices*, **2002**. https://doi.org/10.1023/A:1014683114796.

[24] Nguyen, N. T.; Huang, X. Miniature Valveless Pumps Based on Printed Circuit Board Technique. *Sensors Actuators, A Phys.*, **2001**. https://doi.org/10.1016/S0924-4247(00)00500-8.

[25] Anand, S. S.; Philip, B. K.; Mehendale, H. M. Volatile Organic Compounds. In *Encyclopedia of Toxicology: Third Edition*; 2014. https://doi.org/10.1016/B978-0-12-386454-3.00358-4.

[26] Spokas, K. A.; Novak, J. M.; Stewart, C. E.; Cantrell, K. B.; Uchimiya, M.; DuSaire, M. G.; Ro, K. S. Qualitative Analysis of Volatile Organic Compounds on Biochar. *Chemosphere*, **2011**. https://doi.org/10.1016/j.chemosphere.2011.06.108.

[27] Berenjian, A.; Chan, N.; Malmiri, H. J. Volatile Organic Compounds Removal Methods: A Review. *American Journal of Biochemistry and Biotechnology*. 2012. https://doi.org/10.3844/ajbbsp.2012.220.229.

[28] Li, X.; Zhang, L.; Yang, Z.; He, Z.; Wang, P.; Yan, Y.; Ran, J. Hydrophobic Modified Activated Carbon Using PDMS for the Adsorption of VOCs in Humid Condition. *Sep. Purif. Technol.*, **2020**, *239* (October 2019), 116517. https://doi.org/10.1016/j.seppur.2020.116517.

[29] Troughton, M. J. *Polycarbonate*; William Andrew Publishing, 2009. https://doi.org/10.1016/B978-0-8155-1581-4.50029-9.

[30] Hasegawa, M.; Horie, K. Photophysics, Photochemistry, and Optical Properties of Polyimides. *Prog. Polym. Sci.*, **2001**, *26* (2), 259–335. https://doi.org/10.1016/S0079-6700(00)00042-3.

[31] Xiao, M.; Sun, L.; Liu, J.; Li, Y.; Gong, K. Synthesis and Properties of Polystyrene/Graphite Nanocomposites. *Polymer (Guildf).*, **2002**, *43* (8), 2245–2248. https://doi.org/10.1016/S0032-3861(02)00022-8.

[32] Li, J. H.; Hong, R. Y.; Li, M. Y.; Li, H. Z.; Zheng, Y.; Ding, J. Effects of ZnO Nanoparticles on the Mechanical and Antibacterial Properties of Polyurethane Coatings. *Prog. Org. Coatings*, **2009**, *64* (4), 504–509. https://doi.org/10.1016/J.PORGCOAT.2008.08.013.

[33] Chini, S. F.; Amirfazli, A. Understanding Pattern Collapse in Photolithography Process Due to Capillary Forces. *Langmuir*, **2010**, *26* (16), 13707–13714. https://doi.org/10.1021/la101521k.

[34] Kumar, A.; Gupta, A.; Kant, R.; Akhtar, S. N.; Tiwari, N.; Ramkumar, J.; Bhattacharya, S. Optimization of Laser Machining Process for the Preparation of Photomasks, and Its Application to Microsystems Fabrication. *J. Micro/Nanolithography, MEMS, MOEMS*, **2013**, *12* (4), 041203.

[35] Gupta, A.; Sundriyal, P.; Basu, A.; Manoharan, K.; Kant, R.; Bhattacharya, S. Nano-Finishing of MEMS-Based Platforms for Optimum Optical Sensing. *J. Micromanufacturing*, **2020**, *3* (1), 39–53.

[36] Wang, C. H.; Lee, G. Bin. Pneumatically Driven Peristaltic Micropumps Utilizing Serpentine-Shape Channels. *J. Micromechanics Microengineering*, **2006**, *16* (2), 341–348. https://doi.org/10.1088/0960-1317/16/2/019.

[37] Kokkoris, G.; Tserepi, A.; Boudouvis, A. G.; Gogolides, E. Simulation of SiO2 and Si Feature Etching for Microelectronics and Microelectromechanical Systems Fabrication: A Combined Simulator Coupling Modules of Surface Etching, Local Flux Calculation, and Profile Evolution. *J. Vac. Sci. Technol. A Vacuum, Surfaces, Film.*, **2004**, *22* (4), 1896–1902. https://doi.org/10.1116/1.1738660.

[38] Unger, M. A.; Chou, H.; Thorsen, T.; Scherer, A.; Stephen, R.; Unger, M. A.; Chou, H.; Thorsen, T.; Scherer, A.; Quake, S. R. Linked References Are Available on JSTOR for This Article : Valves and Pumps by Multilayer Soft Lithography. **2016**, *288* (5463), 113–116.

[39] Yilgör, E.; Yilgör, I. Silicone Containing Copolymers: Synthesis, Properties and Applications. *Prog. Polym. Sci.*, **2014**, *39* (6), 1165–1195. https://doi.org/10.1016/j.progpolymsci.2013.11.003.

[40] Mondal, K.; Balasubramaniam, B.; Gupta, A.; Lahcen, A. A.; Kwiatkowski, M. Carbon Nanostructures for Energy and Sensing Applications. *J. Nanotechnol.*, **2019**, *2019*, 10–13. https://doi.org/10.1155/2019/1454327.

[41] Gupta, A.; Gangopadhyay, S.; Gangopadhyay, K.; Bhattacharya, S. Palladium-Functionalized

Nanostructured Platforms for Enhanced Hydrogen Sensing. *Nanomater. Nanotechnol.*, **2016**, *6*. https://doi.org/10.5772/63987.

[42] Gupta, A.; Srivastava, A.; Mathai, C. J.; Gangopadhyay, K.; Gangopadhyay, S.; Bhattacharya, S. Nano Porous Palladium Sensor for Sensitive and Rapid Detection of Hydrogen. *Sens. Lett.*, **2014**, *12* (8), 1279–1285. https://doi.org/10.1166/sl.2014.3307.

[43] Gupta, A.; Parida, P. K.; Pal, P. Functional Films for Gas Sensing Applications : A Review. In *Sensors for Automotive and Aerospace Applications*; Springer Singapore, 2019; pp 7–37. https://doi.org/10.1007/978-981-13-3290-6.

[44] Brittain, S.; Paul, K.; Zhao, X. M.; Whitesides, G. Soft Lithography and Microfabrication. *Phys. World*, **1998**, *11* (5), 31–36. https://doi.org/10.1088/2058-7058/11/5/30.

[45] Hale, P. S.; Kappen, P.; Prissanaroon, W.; Brack, N.; Pigram, P. J.; Liesegang, J. Minimizing Silicone Transfer during Micro-Contact Printing. *Appl. Surf. Sci.*, **2007**, *253* (8), 3746–3750. https://doi.org/10.1016/j.apsusc.2005.04.060.

[46] Man, P. F.; Jones, D. K.; Mastrangelo, C. H. Microfluidic Plastic Capillaries on Silicon Substrates: A New Inexpensive Technology for Bioanalysis Chips. In *Proceedings of the IEEE Micro Electro Mechanical Systems (MEMS)*; 1997. https://doi.org/10.1109/memsys.1997.581840.

[47] Kim, E.; Xia, Y.; Whitesides, G. M. Micromolding in Capillaries: Applications in Materials Science. *J. Am. Chem. Soc.*, **1996**, *118* (24), 5722–5731. https://doi.org/10.1021/ja960151v.

[48] Whitesides, G. M.; Ostuni, E.; Takayama, S.; Jiang, X.; Ingber, D. E. Soft Lithography in Biology and Biochemistry. *Annu. Rev. Biomed. Eng.*, **2001**, *3*, 335–373. https://doi.org/10.1146/ANNUREV.BIOENG.3.1.335.

[49] Whitesides, G. M.; Christopher Love, J. The Art of Building Small. *Sci. Am.*, **2001**, *285* (3), 38–47. https://doi.org/10.1038/SCIENTIFICAMERICAN0901-38.

[50] Lee, J. H.; Kim, C. H.; Ho, K. M.; Constant, K. Two-Polymer Microtransfer Molding for Highly Layered Microstructures. *Adv. Mater.*, **2005**, *17* (20), 2481–2485. https://doi.org/10.1002/adma.200500721.

[51] Zhao, X. M.; Xia, Y.; Whitesides, G. M. Fabrication of Three-Dimensional Micro-Structures: Microtransfer Molding. *Adv. Mater.*, **1996**, *8* (10), 837–840. https://doi.org/10.1002/ADMA.19960081016.

[52] Chan, E. K. L.; Wong, C. K. Y.; Lee, M.; Yuen, M. M. F.; Lee, Y. K. Using PDMS Micro-Transfer Moulding for Polymer Flip Chip Packaging on MEMS. *Proc. - Electron. Components Technol. Conf.*, **2005**, *2*, 1071–1076. https://doi.org/10.1109/ECTC.2005.1441404.

[53] Liyu, D.; Nemati, S. H.; Vasdekis, A. E. Solvent-Assisted Prototyping of Microfluidic and Optofluidic Microsystems in Polymers. *J. Polym. Sci. Part B Polym. Phys.*, **2016**, *54* (17), 1681–1686. https://doi.org/10.1002/polb.24091.

[54] Radha, B.; Kulkarni, G. U. Micromolding-a Soft Lithography Technique. *Micromanufacturing Process.*, **2016**, No. October 2016, 329–347. https://doi.org/10.1201/b13020-25.

[55] Katare, P.; Gorthi, S. S. Microwave Irradiation-Based Rapid Curing of PDMS for Microfluidic Applications. *Microfluidics and Nanofluidics*. 2020. https://doi.org/10.1007/s10404-020-02348-0.

[56] Basinger et al. States Patent [Â »]. *Search*, **2018**, *2*.

[57] Rogers, J. A. Generating ~90 Nanometer Features Using Near-Field Contact-Mode Photolithography with an Elastomeric Phase Mask. *J. Vac. Sci. Technol. B Microelectron. Nanom. Struct.*, **1998**, *16* (1), 59. https://doi.org/10.1116/1.589836.

[58] Paik, S.; Kim, G.; Chang, S.; Lee, S.; Jin, D.; Jeong, K. Y.; Lee, I. S.; Lee, J.; Moon, H.; Lee, J.; et al. Near-Field Sub-Diffraction Photolithography with an Elastomeric Photomask. *Nat. Commun.*, **2020**, *11* (1), 1–13. https://doi.org/10.1038/s41467-020-14439-1.

[59] SadAbadi, H.; Badilescu, S.; Packirisamy, M.; Wüthrich, R. Integration of Gold Nanoparticles in PDMS Microfluidics for Lab-on-a-Chip Plasmonic Biosensing of Growth Hormones. *Biosens. Bioelectron.*, **2013**, *44* (1), 77–84. https://doi.org/10.1016/J.BIOS.2013.01.016.

[60] Chen, J.; Zhu, Y.; Jiang, W. A Stretchable and Transparent Strain Sensor Based on Sandwich-like PDMS / CNTs / PDMS Composite Containing an Ultrathin Conductive CNT Layer. *Compos. Sci. Technol.*, **2020**, *186* (September 2019), 107938. https://doi.org/10.1016/j.compscitech.2019.107938.

[61] Lee, M. H.; Huntington, M. D.; Zhou, W.; Yang, J.; Odom, T. W. Programmable Soft Lithography : Solvent-Assisted. *nano Lett.*, **2011**, 311–315. https://doi.org/10.1021/nl102206x.

[62] Blattmann, C. O.; Pratsinis, S. E. Single-Step Fabrication of Polymer Nanocomposite Films. *Materials (Basel).*, **2018**, *11* (7). https://doi.org/10.3390/MA11071177.

[63] Ataollahi, F.; Pramanik, S.; Moradi, A.; Dalilottojari, A.; Pingguan-Murphy, B.; Wan Abas, W. A. B.; Abu Osman, N. A. Endothelial Cell Responses in Terms of Adhesion, Proliferation, and Morphology to Stiffness of Polydimethylsiloxane Elastomer Substrates. *J. Biomed. Mater. Res. A*, **2015**, *103* (7), 2203–2213. https://doi.org/10.1002/JBM.A.35186.

[64] Park, M.; Park, J.; Jeong, U. Design of Conductive Composite Elastomers for Stretchable Electronics. *undefined*, **2014**, *9* (2), 244–260. https://doi.org/10.1016/J.NANTOD.2014.04.009.

[65] Chun, K. Y.; Oh, Y.; Rho, J.; Ahn, J. H.; Kim, Y. J.; Choi, H. R.; Baik, S. Highly Conductive, Printable and Stretchable Composite Films of Carbon Nanotubes and Silver. *Nat. Nanotechnol.*, **2010**, *5* (12), 853–857. https://doi.org/10.1038/NNANO.2010.232.

[66] Chu, K.; Kim, D.; Sohn, Y.; Lee, S.; Moon, C.; Park, S. Electrical and Thermal Properties of Carbon-Nanotube Composite for Flexible Electric Heating-Unit Applications. *IEEE Electron Device Lett.*, **2013**, *34* (5), 668–670. https://doi.org/10.1109/LED.2013.2249493.

[67] Kim, J. A.; Lee, S. H.; Park, H.; Kim, J. H.; Park, T. H. Microheater Based on Magnetic Nanoparticle Embedded PDMS. *Nanotechnology*, **2010**, *21* (16), 165102. https://doi.org/10.1088/0957-4484/21/16/165102.

[68] Fortin, J. P.; Wilhelm, C.; Servais, J.; Ménager, C.; Bacri, J. C.; Gazeau, F. Size-Sorted Anionic Iron Oxide Nanomagnets as Colloidal Mediators for Magnetic Hyperthermia. *J. Am. Chem. Soc.*, **2007**, *129* (9), 2628–2635. https://doi.org/10.1021/JA067457E.

[69] Sun, J.; Zhuang, J.; Shi, J.; Kormakov, S.; Liu, Y.; Yang, Z.; Wu, D. Highly Elastic and Ultrathin Nanopaper-Based Nanocomposites with Superior Electric and Thermal Characteristics. *J. Mater. Sci.*, **2019**, *54* (11), 8436–8449. https://doi.org/10.1007/s10853-019-03472-1.

[70] Coleman, J. N.; Khan, U.; Blau, W. J.; Gun'ko, Y. K. Small but Strong: A Review of the Mechanical Properties of Carbon Nanotube-Polymer Composites. *Carbon N. Y.*, **2006**, *44* (9), 1624–1652. https://doi.org/10.1016/j.carbon.2006.02.038.

[71] Sun, J.; Shen, J.; Chen, S.; Cooper, M. A.; Fu, H.; Wu, D.; Yang, Z. Nanofiller Reinforced Biodegradable PLA/PHA Composites: Current Status and Future Trends. *Polymers (Basel).*, **2018**, *10* (5), 1–22. https://doi.org/10.3390/polym10050505.

[72] Sun, J.; Zhao, Y.; Yang, Z.; Shen, J.; Cabrera, E.; Lertola, M. J.; Yang, W.; Zhang, D.; Benatar, A.; Castro, J. M.; et al. Highly Stretchable and Ultrathin Nanopaper Composites for Epidermal Strain Sensors. *Nanotechnology*, **2018**, *29* (35), 0–27. https://doi.org/10.1088/1361-6528/aacc59.

[73] Chen, M. J.; Shao, Z. B.; Wang, X. L.; Chen, L.; Wang, Y. Z. Halogen-Free Flame-Retardant Flexible Polyurethane Foam with a Novel Nitrogen-Phosphorus Flame Retardant. *Ind. Eng. Chem. Res.*, **2012**. https://doi.org/10.1021/ie301004d.

[74] Zhu, D.; Handschuh-Wang, S.; Zhou, X. *Recent Progress in Fabrication and Application of Polydimethylsiloxane Sponges*; 2017; Vol. 5. https://doi.org/10.1039/c7ta04577h.

[75] Zhao, X.; Li, L.; Li, B.; Zhang, J.; Wang, A. Durable Superhydrophobic/Superoleophilic PDMS Sponges and Their Applications in Selective Oil Absorption and in Plugging Oil Leakages. *J. Mater. Chem. A*, **2014**, *2* (43), 18281–18287. https://doi.org/10.1039/c4ta04406a.

[76] Hamdani, S.; Longuet, C.; Perrin, D.; Lopez-cuesta, J. M.; Ganachaud, F. Flame Retardancy of Silicone-Based Materials. *Polym. Degrad. Stab.*, **2009**, *94* (4), 465–495. https://doi.org/10.1016/j.polymdegradstab.2008.11.019.

[77] Tang, L. C.; Wang, X.; Gong, L. X.; Peng, K.; Zhao, L.; Chen, Q.; Wu, L. Bin; Jiang, J. X.; Lai, G. Q. Creep and Recovery of Polystyrene Composites Filled with Graphene Additives. *Compos. Sci. Technol.*, **2014**, *91*, 63–70. https://doi.org/10.1016/j.compscitech.2013.11.028.

[78] Gong, L. X.; Zhao, L.; Tang, L. C.; Liu, H. Y.; Mai, Y. W. Balanced Electrical, Thermal and Mechanical Properties of Epoxy Composites Filled with Chemically Reduced Graphene Oxide and Rubber Nanoparticles. *Compos. Sci. Technol.*, **2015**, *121*, 104–114. https://doi.org/10.1016/j.compscitech.2015.10.023.

[79] Gong, L. X.; Pei, Y. B.; Han, Q. Y.; Zhao, L.; Wu, L. Bin; Jiang, J. X.; Tang, L. C. Polymer Grafted Reduced Graphene Oxide Sheets for Improving Stress Transfer in Polymer Composites. *Compos. Sci. Technol.*, **2016**, *134*, 144–152. https://doi.org/10.1016/j.compscitech.2016.08.014.

[80] Wu, S.; Zhang, J.; Ladani, R. B.; Ravindran, A. R.; Mouritz, A. P.; Kinloch, A. J.; Wang, C. H. Novel Electrically Conductive Porous PDMS / Carbon Nanofi Ber Composites for Deformable Strain Sensors and Conductors. *Appl. materails interfaces*, **2017**, 3–11. https://doi.org/10.1021/acsami.7b00847.

[81] Rivero, P. J.; Goicoechea, J.; Urrutia, A.; Matias, I. R.; Arregui, F. J. Multicolor Layer-by-Layer Films Using Weak Polyelectrolyte Assisted Synthesis of Silver Nanoparticles. *Nanoscale Res.*

Lett., **2013**, *8* (1), 1–10. https://doi.org/10.1186/1556-276X-8-438/FIGURES/10.

[82] Reincke, F.; Hickey, S. G.; Kegel, W. K.; Vanmaekelbergh, D.; Reincke,] F; Hickey, S. G.; Vanmaekelbergh, P. D.; Kegel, W. K. Spontaneous Assembly of a Monolayer of Charged Gold Nanocrystals at the Water/Oil Interface. *Angew. Chemie Int. Ed.*, **2004**, *43* (4), 458–462. https://doi.org/10.1002/ANIE.200352339.

[83] Lu, G.; Li, H.; Zhang, H. Gold-Nanoparticle-Embedded Polydimethylsiloxane Elastomers for Highly Sensitive Raman Detection. *Small*, **2012**, *8* (9), 1336–1340. https://doi.org/10.1002/SMLL.201102258.

[84] Ozmen, M.; Ertekin, B.; Ersoz, M.; Paunov, V. N. Fabrication of Albumin-Micropatterned Surfaces by Colloidal Microcontact Printing Technique. *RSC Adv.*, **2013**, *3* (26), 10420–10426. https://doi.org/10.1039/C3RA40507A.

[85] Wang, T.; Colver, P. J.; Bon, S. A. F.; Keddie, J. L. Soft Polymer and Nano-Clay Supracolloidal Particles in Adhesives: Synergistic Effects on Mechanical Properties. *Soft Matter*, **2009**, *5* (20), 3842–3849. https://doi.org/10.1039/b904740a.

[86] Shen, M.; Sun, Y.; Xu, J.; Guo, X.; Prud'Homme, R. K. Rheology and Adhesion of Poly(Acrylic Acid)/Laponite Nanocomposite Hydrogels as Biocompatible Adhesives. *Langmuir*, **2014**, *30* (6), 1636–1642. https://doi.org/10.1021/la4045623.

[87] Khan, U.; May, P.; Porwal, H.; Nawaz, K.; Coleman, J. N. Improved Adhesive Strength and Toughness of Polyvinyl Acetate Glue on Addition of Small Quantities of Graphene. *ACS Appl. Mater. Interfaces*, **2013**, *5* (4), 1423–1428. https://doi.org/10.1021/am302864f.

[88] Ramakrishna, S. N.; Clasohm, L. Y.; Rao, A.; Spencer, N. D. Controlling Adhesion Force by Means of Nanoscale Surface Roughness. *Langmuir*, **2011**, *27* (16), 9972–9978. https://doi.org/10.1021/la201727t.

[89] Patil, S.; Malasi, A.; Majumder, A.; Ghatak, A.; Sharma, A. Reusable Antifouling Viscoelastic Adhesive with an Elastic Skin. *Langmuir*, **2012**, *28* (1), 42–46. https://doi.org/10.1021/la203871c.

[90] Patil, S.; Ranjan, A.; Sharma, A. Prefracture Instabilities Govern Generation of Self-Affine Surfaces in Tearing of Soft Viscoelastic Elastomeric Sheets. *Macromolecules*, **2012**, *45* (4), 2066–2073. https://doi.org/10.1021/ma202339y.

[91] Levitt, A. S.; Alhabeb, M.; Hatter, C. B.; Sarycheva, A.; Dion, G.; Gogotsi, Y. Electrospun MXene/Carbon Nanofibers as Supercapacitor Electrodes. *J. Mater. Chem. A*, **2019**. https://doi.org/10.1039/c8ta09810g.

[92] Chen, P.; Yun, Y. S.; Bak, H.; Cho, S. Y.; Jin, H. J. Multiwalled Carbon Nanotubes-Embedded Electrospun Bacterial Cellulose Nanofibers. In *Molecular Crystals and Liquid Crystals*; 2010. https://doi.org/10.1080/15421401003613659.

[93] de Dicastillo, C. L.; Garrido, L.; Alvarado, N.; Romero, J.; Palma, J. L.; Galotto, M. J. Improvement of Polylactide Properties through Cellulose Nanocrystals Embedded in Poly(Vinyl Alcohol) Electrospun Nanofibers. *Nanomaterials*, **2017**. https://doi.org/10.3390/nano7050106.

[94] Mehrasa, M.; Asadollahi, M. A.; Ghaedi, K.; Salehi, H.; Arpanaei, A. Electrospun Aligned PLGA

and PLGA/Gelatin Nanofibers Embedded with Silica Nanoparticles for Tissue Engineering. *Int. J. Biol. Macromol.*, **2015**. https://doi.org/10.1016/j.ijbiomac.2015.05.050.

[95] Wang, T.; Lei, C. H.; Liu, D.; Manea, M.; Asua, J. M.; Creton, C.; Dalton, A. B.; Keddie, J. L. A Molecular Mechanism for Toughening and Strengthening Waterborne Nanocomposites. *Adv. Mater.*, **2008**, *20* (1), 90–94. https://doi.org/10.1002/adma.200700821.

[96] Brown, H. R. Chain Pullout and Mobility Effects in Friction and Lubrication Author (s): H . R . Brown Published by : American Association for the Advancement of Science Stable URL : Http://Www.Jstor.Org/Stable/2883313 Accessed : 03-05-2016 15 : 26 UTC Chain Pullout . **2016**, *263* (5152), 1411–1413.

[97] Gaaz, T. S.; Sulong, A. B.; Akhtar, M. N.; Kadhum, A. A. H.; Mohamad, A. B.; Al-Amiery, A. A.; McPhee, D. J. Properties and Applications of Polyvinyl Alcohol, Halloysite Nanotubes and Their Nanocomposites. *Molecules*, **2015**, *20* (12), 22833–22847. https://doi.org/10.3390/molecules201219884.

[98] Wang, L.; Chen, Y.; Lin, L.; Wang, H.; Huang, X.; Xue, H.; Gao, J. Highly Stretchable , Anti-Corrosive and Wearable Strain Sensors Based on the PDMS / CNTs Decorated Elastomer Nano Fi Ber Composite. *Chem. Eng. J.*, **2019**, *362* (January), 89–98. https://doi.org/10.1016/j.cej.2019.01.014.

[99] El-Tantawy, F.; Kamada, K.; Ohnabe, H. A Novel Way of Enhancing the Electrical and Thermal Stability of Conductive Epoxy Resin-Carbon Black Composites via the Joule Heating Effect for Heating-Element Applications. *J. Appl. Polym. Sci.*, **2003**, *87* (2), 97–109. https://doi.org/10.1002/app.10851.

[100] Huang, N. J.; Zang, J.; Zhang, G. D.; Guan, L. Z.; Li, S. N.; Zhao, L.; Tang, L. C. Efficient Interfacial Interaction for Improving Mechanical Properties of Polydimethylsiloxane Nanocomposites Filled with Low Content of Graphene Oxide Nanoribbons. *RSC Adv.*, **2017**, *7* (36), 22045–22053. https://doi.org/10.1039/c7ra02439h.

[101] Kharaghani, D.; Gitigard, P.; Ohtani, H.; Kim, K. O.; Ullah, S.; Saito, Y.; Khan, M. Q.; Kim, I. S. Design and Characterization of Dual Drug Delivery Based on In-Situ Assembled PVA/PAN Core-Shell Nanofibers for Wound Dressing Application. *Sci. Rep.*, **2019**, *9* (1), 1–11. https://doi.org/10.1038/s41598-019-49132-x.

[102] Yan, F.; Zhang, X.; Liu, F.; Li, X.; Zhang, Z. Adjusting the Properties of Silicone Rubber Filled with Nanosilica by Changing the Surface Organic Groups of Nanosilica. *Compos. Part B Eng.*, **2015**, *75*, 47–52. https://doi.org/10.1016/j.compositesb.2015.01.030.

[103] Gaharwar, A. K.; Peppas, N. A.; Khademhosseini, A. Nanocomposite Hydrogels for Biomedical Applications. *Biotechnol. Bioeng.*, **2014**. https://doi.org/10.1002/bit.25160.

[104] Yin, J.; Deng, B. Polymer-Matrix Nanocomposite Membranes for Water Treatment. *Journal of Membrane Science*. 2015. https://doi.org/10.1016/j.memsci.2014.11.019.

[105] Papageorgiou, D. G.; Kinloch, I. A.; Young, R. J. Mechanical Properties of Graphene and Graphene-Based Nanocomposites. *Progress in Materials Science*. 2017. https://doi.org/10.1016/j.pmatsci.2017.07.004.

[106] Kokabi, M.; Sirousazar, M.; Hassan, Z. M. PVA-Clay Nanocomposite Hydrogels for Wound Dressing. *Eur. Polym. J.*, **2007**. https://doi.org/10.1016/j.eurpolymj.2006.11.030.

[107] Mittal, V. *Optimization of Polymer Nanocomposite Properties*; 2010. https://doi.org/10.1002/9783527629275.

[108] Cioffi, N.; Torsi, L.; Ditaranto, N.; Tantillo, G.; Ghibelli, L.; Sabbatini, L.; Bleve-Zacheo, T.; D'Alessio, M.; Zambonin, P. G.; Traversa, E. Copper Nanoparticle/Polymer Composites with Antifungal and Bacteriostatic Properties. *Chem. Mater.*, **2005**. https://doi.org/10.1021/cm0505244.

[109] Zou, H.; Wu, S.; Shen, J. Polymer/Silica Nanocomposites: Preparation, Characterization, Propertles, and Applications. *Chemical Reviews*. 2008. https://doi.org/10.1021/cr068035q.

[110] Beecroft, L. L.; Ober, C. K. Nanocomposite Materials for Optical Applications. *Chemistry of Materials*. 1997. https://doi.org/10.1021/cm960441a.

[111] Jeong, B. H.; Hoek, E. M. V.; Yan, Y.; Subramani, A.; Huang, X.; Hurwitz, G.; Ghosh, A. K.; Jawor, A. Interfacial Polymerization of Thin Film Nanocomposites: A New Concept for Reverse Osmosis Membranes. *J. Memb. Sci.*, **2007**. https://doi.org/10.1016/j.memsci.2007.02.025.

[112] Haraguchi, K. Nanocomposite Hydrogels. *Current Opinion in Solid State and Materials Science*. 2007. https://doi.org/10.1016/j.cossms.2008.05.001.

[113] Lee, L. J.; Zeng, C.; Cao, X.; Han, X.; Shen, J.; Xu, G. Polymer Nanocomposite Foams. *Compos. Sci. Technol.*, **2005**. https://doi.org/10.1016/j.compscitech.2005.06.016.

[114] Yang, D. Application of Nanocomposites for Supercapacitors: Characteristics and Properties. In *Nanocomposites - New Trends and Developments*; 2012. https://doi.org/10.5772/50409.

[115] Croce, F.; Appetecchi, G. B.; Persi, L.; Scrosati, B. Nanocomposite Polymer Electrolytes for Lithium Batteries. *Nature*, **1998**. https://doi.org/10.1038/28818.

[116] Al-Naamani, L.; Dobretsov, S.; Dutta, J. Chitosan-Zinc Oxide Nanoparticle Composite Coating for Active Food Packaging Applications. *Innov. Food Sci. Emerg. Technol.*, **2016**. https://doi.org/10.1016/j.ifset.2016.10.010.

[117] Cao, Y.; Li, G.; Li, X. Graphene/Layered Double Hydroxide Nanocomposite: Properties, Synthesis, and Applications. *Chemical Engineering Journal*. 2016. https://doi.org/10.1016/j.cej.2016.01.114.

[118] Kowalczyk, M.; Piorkowska, E.; Kulpinski, P.; Pracella, M. Mechanical and Thermal Properties of PLA Composites with Cellulose Nanofibers and Standard Size Fibers. *Compos. Part A Appl. Sci. Manuf.*, **2011**. https://doi.org/10.1016/j.compositesa.2011.07.003.

[119] Nguyen-Tri, P.; Nguyen, T. A.; Carriere, P.; Ngo Xuan, C. Nanocomposite Coatings: Preparation, Characterization, Properties, and Applications. *Int. J. Corros.*, **2018**. https://doi.org/10.1155/2018/4749501.

[120] Rafiee, M. A.; Rafiee, J.; Wang, Z.; Song, H.; Yu, Z. Z.; Koratkar, N. Enhanced Mechanical Properties of Nanocomposites at Low Graphene Content. *ACS Nano*, **2009**. https://doi.org/10.1021/nn9010472.

[121] Roy, M.; Nelson, J. K.; MacCrone, R. K.; Schadler, L. S.; Reed, C. W.; Keefe, R.; Zenger, W. Polymer Nanocomposite Dielectrics - The Role of the Interface. *IEEE Trans. Dielectr. Electr. Insul.*, **2005**. https://doi.org/10.1109/TDEI.2005.1511089.

[122] Cyras, V. P.; Manfredi, L. B.; Ton-That, M. T.; Vázquez, A. Physical and Mechanical Properties of Thermoplastic Starch/Montmorillonite Nanocomposite Films. *Carbohydr. Polym.*, **2008**. https://doi.org/10.1016/j.carbpol.2007.11.014.

[123] Croce, F.; Curini, R.; Martinelli, A.; Persi, L.; Ronci, F.; Scrosati, B.; Caminiti, R. Physical and Chemical Properties of Nanocomposite Polymer Electrolytes. *J. Phys. Chem. B*, **1999**. https://doi.org/10.1021/jp992307u.

[124] M. Reda, S.; M. Al-Ghannam, S. Synthesis and Electrical Properties of Polyaniline Composite with Silver Nanoparticles. *Adv. Mater. Phys. Chem.*, **2012**. https://doi.org/10.4236/ampc.2012.22013.

[125] Nelson, J. K.; Hu, Y. Nanocomposite Dielectrics - Properties and Implications. In *Journal of Physics D: Applied Physics*; 2005. https://doi.org/10.1088/0022-3727/38/2/005.

[126] Deng, S. B.; Liao, W.; Yang, J. C.; Cao, Z. J.; Wang, Y. Z. Flame-Retardant and Smoke-Suppressed Silicone Foams with Chitosan-Based Nanocoatings. *Ind. Eng. Chem. Res.*, **2016**, *55* (27), 7239–7248. https://doi.org/10.1021/acs.iecr.6b00532.

[127] Yang, J.; Han, C. R.; Duan, J. F.; Xu, F.; Sun, R. C. Mechanical and Viscoelastic Properties of Cellulose Nanocrystals Reinforced Poly(Ethylene Glycol) Nanocomposite Hydrogels. *ACS Appl. Mater. Interfaces*, **2013**. https://doi.org/10.1021/am4001997.

[128] Klangmuang, P.; Sothornvit, R. Barrier Properties, Mechanical Properties and Antimicrobial Activity of Hydroxypropyl Methylcellulose-Based Nanocomposite Films Incorporated with Thai Essential Oils. *Food Hydrocoll.*, **2016**. https://doi.org/10.1016/j.foodhyd.2016.06.018.

[129] Liu, J.; Ye, L.; Wooh, S.; Kappl, M.; Steffen, W.; Butt, H. J. Optimizing Hydrophobicity and Photocatalytic Activity of PDMS-Coated Titanium Dioxide. *ACS Appl. Mater. Interfaces*, **2019**, *11* (30), 27422–27425. https://doi.org/10.1021/acsami.9b07490.

[130] Kim, J.; Chaudhury, M. K.; Owen, M. J. Hydrophobicity Loss and Recovery of Silicone HV Insulation. *IEEE Trans. Dielectr. Electr. Insul.*, **1999**. https://doi.org/10.1109/94.798126.

[131] Wang, L.; Sun, B.; Ziemer, K. S.; Barabino, G. A.; Carrier, R. L. Chemical and Physical Modifications to Poly(Dimethylsiloxane) Surfaces Affect Adhesion of Caco-2 Cells. *J. Biomed. Mater. Res. - Part A*, **2010**. https://doi.org/10.1002/jbm.a.32621.

[132] Bongaerts, J. H. H.; Fourtouni, K.; Stokes, J. R. Soft-Tribology: Lubrication in a Compliant PDMS-PDMS Contact. *Tribol. Int.*, **2007**. https://doi.org/10.1016/j.triboint.2007.01.007.

[133] Zhou, J.; Ellis, A. V.; Voelcker, N. H. Recent Developments in PDMS Surface Modification for Microfluidic Devices. *Electrophoresis*. 2010. https://doi.org/10.1002/elps.200900475.

[134] Hillborg, H.; Gedde, U. W. Hydrophobicity Recovery of Polydimethylsiloxane after Exposure to Corona Discharges. *Polymer (Guildf).*, **1998**. https://doi.org/10.1016/S0032-3861(97)00484-9.

[135] Chuah, Y. J.; Koh, Y. T.; Lim, K.; Menon, N. V.; Wu, Y.; Kang, Y. Simple Surface Engineering of Polydimethylsiloxane with Polydopamine for Stabilized Mesenchymal Stem Cell Adhesion and Multipotency. *Sci. Rep.*, **2015**. https://doi.org/10.1038/srep18162.

[136] Konaka, R.; Kasahara, E.; Dunlap, W. C.; Yamamoto, Y.; Chien, K. C.; Inoue, M. Irradiation of Titanium Dioxide Generates Both Singlet Oxygen and Superoxide Anion. *Free Radic. Biol. Med.*, **1999**, *27* (3–4), 294–300. https://doi.org/10.1016/S0891-5849(99)00050-7.

[137] Zarifi, M. H.; Farsinezhad, S.; Abdolrazzaghi, M.; Daneshmand, M.; Shankar, K. Selective Microwave Sensors Exploiting the Interaction of Analytes with Trap States in TiO2 Nanotube Arrays. *Nanoscale*, **2016**, *8* (14), 7466–7473. https://doi.org/10.1039/c5nr06567d.

[138] Hillborg, H.; Gedde, U. W. Hydrophobicity Changes in Silicone Rubbers. *IEEE Trans. Dielectr. Electr. Insul.*, **1999**. https://doi.org/10.1109/94.798127.

[139] van Meer, B. J.; de Vries, H.; Firth, K. S. A.; van Weerd, J.; Tertoolen, L. G. J.; Karperien, H. B. J.; Jonkheijm, P.; Denning, C.; IJzerman, A. P.; Mummery, C. L. Small Molecule Absorption by PDMS in the Context of Drug Response Bioassays. *Biochem. Biophys. Res. Commun.*, **2017**. https://doi.org/10.1016/j.bbrc.2016.11.062.

[140] Gökaltun, A.; Kang, Y. B. (Abraham); Yarmush, M. L.; Usta, O. B.; Asatekin, A. Simple Surface Modification of Poly(Dimethylsiloxane) via Surface Segregating Smart Polymers for Biomicrofluidics. *Sci. Rep.*, **2019**. https://doi.org/10.1038/s41598-019-43625-5.

[141] Bernardo, P.; Drioli, E.; Golemme, G. Membrane Gas Separation: A Review/State of the Art. *Ind. Eng. Chem. Res.*, **2009**, *48* (10), 4638–4663. https://doi.org/10.1021/ie8019032.

[142] Anderson, M. R.; Mattes, B. R.; Reiss, H. GAS SEPARATION MEMBRANES : A NOVEL APPLICATION FOR CONDUCTING POLYMERS. *Synth. Met.*, **1991**, *43*, 1151–1154. https://doi.org/10.1016/0379-6779(91)91575-U.

[143] Roberts, D. L.; Chlngt, G. D. Recovery of Freon Gases with Silicone Rubber Membranes. *Ind. Eng. Chem. Process Des. Dev.*, **1986**, *25* (4), 971–973. https://doi.org/10.1021/i200035a022.

[144] Berean, K. J.; Ou, J. Z.; Nour, M.; Field, M. R.; Alsaif, M. M. Y. A.; Wang, Y.; Ramanathan, R.; Bansal, V.; Kentish, S.; Doherty, C. M.; et al. Enhanced Gas Permeation through Graphene Nanocomposites. *J. Phys. Chem. C*, **2015**. https://doi.org/10.1021/acs.jpcc.5b02995.

[145] Nour, M.; Berean, K.; Balendhran, S.; Ou, J. Z.; Plessis, J. Du; McSweeney, C.; Bhaskaran, M.; Sriram, S.; Kalantar-zadeh, K. CNT/PDMS Composite Membranes for H2 and CH4 Gas Separation. *Int. J. Hydrogen Energy*, **2013**, *38* (25), 10494–10501. https://doi.org/10.1016/j.ijhydene.2013.05.162.

[146] Nour, M.; Berean, K.; Griffin, M. J.; Matthews, G. I.; Bhaskaran, M.; Sriram, S.; Kalantar-Zadeh, K. Nanocomposite Carbon-PDMS Membranes for Gas Separation. *Sensors Actuators, B Chem.*, **2012**, *161* (1), 982–988. https://doi.org/10.1016/j.snb.2011.11.079.

[147] Firpo, G.; Angeli, E.; Repetto, L.; Valbusa, U. Permeability Thickness Dependence of Polydimethylsiloxane (PDMS) Membranes. *J. Memb. Sci.*, **2015**, *481*, 1–8. https://doi.org/10.1016/j.memsci.2014.12.043.

[148] Hwang, I.; Kim, Y.; Kim, S.; Ju, B.; Lee, J. A Facile Fabrication of Semiconductor Nanowires Gas Sensor Using PDMS Patterning and Solution Deposition &. *Sensors Actuators B Chem.*, **2009**, *136*, 224–229. https://doi.org/10.1016/j.snb.2008.10.042.

[149] Gao, Z.; Song, G.; Zhang, X.; Li, Q.; Yang, S.; Wang, T.; Li, Y.; Zhang, L.; Guo, L.; Fu, Y. A Facile PDMS Coating Approach to Room-Temperature Gas Sensors with High Humidity Resistance and Long-Term Stability. *Sensors Actuators B . Chem.*, **2020**, *325*, 128810. https://doi.org/10.1016/j.snb.2020.128810.

[150] He, H.; Zhang, M.; Zhao, T.; Zeng, H.; Xing, L. A Self-Powered Gas Sensor Based on PDMS / Ppy Triboelectric-Gas-Sensing Arrays for the Real-Time Monitoring of Automotive Exhaust Gas at Room. *Sci. China Mater.*, **2019**, *62* (10), 1433–1444. https://doi.org/10.1007/s40843-019-9445-9.

[151] Zhou, T.; Dong, W.; Qiu, Y.; Chen, S.; Wang, X.; Xie, C.; Zeng, D. Selectivity of a ZnO @ ZIF-71 @ PDMS Nanorod Array Gas Sensor Enhanced by Coating a Polymer Selective Separation Membrane. *ACS Appl. Mater. Interfaces*, **2021**, *13*, 54589–54596. https://doi.org/10.1021/acsami.1c16637.

[152] Nam, Y.; Yoo, I.; Yarimaga, O.; Park, I. S.; Park, D.; Song, S.; Kim, J.; Lee, C. W. Photochromic Spiropyran-Embedded PDMS for Highly Sensitive and Tunable Optochemical Gas Sensing. *Chem. Commun.*, **2014**, *50*, 4251–4254. https://doi.org/10.1039/c4cc00567h.

[153] Jeong, Y. R.; Park, H.; Jin, S. W.; Hong, S. Y.; Lee, S. S.; Ha, J. S. Highly Stretchable and Sensitive Strain Sensors Using Fragmentized Graphene Foam. *Adv. Funct. Mater.*, **2015**. https://doi.org/10.1002/adfm.201501000.

[154] Gerlach, C.; Krumm, D.; Illing, M.; Lange, J.; Kanoun, O.; Odenwald, S.; Hubler, A. Printed MWCNT-PDMS-Composite Pressure Sensor System for Plantar Pressure Monitoring in Ulcer Prevention. *IEEE Sens. J.*, **2015**. https://doi.org/10.1109/JSEN.2015.2392084.

[155] Park, M.; Kim, H.; Youngblood, J. P. Strain-Dependent Electrical Resistance of Multi-Walled Carbon Nanotube/Polymer Composite Films. *Nanotechnology*, **2008**. https://doi.org/10.1088/0957-4484/19/05/055705.

[156] Fu, X.; Ramos, M.; Al-Jumaily, A. M.; Meshkinzar, A.; Huang, X. Stretchable Strain Sensor Facilely Fabricated Based on Multi-Wall Carbon Nanotube Composites with Excellent Performance. *J. Mater. Sci.*, **2019**. https://doi.org/10.1007/s10853-018-2954-4.

[157] Huang, K.; Ning, H.; Hu, N.; Liu, F.; Wu, X.; Wang, S.; Liu, Y.; Zou, R.; Yuan, W.; Alamusi; et al. Ultrasensitive MWCNT/PDMS Composite Strain Sensor Fabricated by Laser Ablation Process. *Compos. Sci. Technol.*, **2020**, *192* (March), 108105. https://doi.org/10.1016/j.compscitech.2020.108105.

[158] Li, Y. Q.; Huang, P.; Zhu, W. Bin; Fu, S. Y.; Hu, N.; Liao, K. Flexible Wire-Shaped Strain Sensor from Cotton Thread for Human Health and Motion Detection. *Sci. Rep.*, **2017**. https://doi.org/10.1038/srep45013.

[159] Khan, S.; Tinku, S.; Lorenzelli, L.; Dahiya, R. S. Flexible Tactile Sensors Using Screen-Printed P(VDF-TrFE) and MWCNT/PDMS Composites. *IEEE Sens. J.*, **2015**. https://doi.org/10.1109/JSEN.2014.2368989.

[160] Wang, B.; Lee, B. K.; Kwak, M. J.; Lee, D. W. Graphene/Polydimethylsiloxane Nanocomposite Strain Sensor. *Rev. Sci. Instrum.*, **2013**. https://doi.org/10.1063/1.4826496.

[161] Hassan, G.; Bae, J.; Hassan, A.; Ali, S.; Lee, C. H.; Choi, Y. Ink-Jet Printed Stretchable Strain Sensor Based on Graphene / ZnO Composite on Micro-Random Ridged PDMS Substrate. *Composites*, **2018**. https://doi.org/10.1016/j.compositesa.2018.01.031.

[162] Luo, R.; Li, H.; Du, B.; Zhou, S.; Zhu, Y. A Simple Strategy for High Stretchable , Fl Exible and Conductive Polymer Fi Lms Based on PEDOT : PSS-PDMS Blends. *Org. Electron.*, **2020**, *76* (August 2019), 105451. https://doi.org/10.1016/j.orgel.2019.105451.

[163] Rajitha, G.; Dash, R. K. Optically Transparent and High Dielectric Constant Reduced Graphene Oxide (RGO)-PDMS Based Flexible Composite for Wearable and Flexible Sensors. *Sensors Actuators A. Phys.*, **2018**. https://doi.org/10.1016/j.sna.2018.04.040.

[164] Shi, G.; Lowe, S. E.; Teo, A. J. T.; Dinh, T. K.; Hwa, S.; Qin, J.; Zhang, Y.; Lin, Y.; Zhao, H. A Versatile PDMS Submicrobead / Graphene Oxide Nanocomposite Ink for the Direct Ink Writing of Wearable Micron-Scale Tactile Sensors. *Appl. Mater. Today*, **2019**, *16*, 482–492. https://doi.org/10.1016/j.apmt.2019.06.016.

[165] Risau, W.; Wolburg, H. Development of the Blood-Brain Barrier. *Trends Neurosci.*, **1990**, *13* (5), 174–178. https://doi.org/10.1016/0166-2236(90)90043-A.

[166] van der Helm, M. W.; van der Meer, A. D.; Eijkel, J. C. T.; van den Berg, A.; Segerink, L. I. Microfluidic Organ-on-Chip Technology for Blood-Brain Barrier Research. *Tissue Barriers*, **2016**, *4* (1). https://doi.org/10.1080/21688370.2016.1142493.

[167] Abbott, N. J.; Patabendige, A. A. K.; Dolman, D. E. M.; Yusof, S. R.; Begley, D. J. Structure and Function of the Blood-Brain Barrier. *Neurobiol. Dis.*, **2010**, *37* (1), 13–25. https://doi.org/10.1016/j.nbd.2009.07.030.

[168] Engelhardt, B. Development of the Blood-Brain Barrier. *Cell and Tissue Research*. 2003. https://doi.org/10.1007/s00441-003-0751-z.

[169] Sooriyaarachchi, D.; Zhou, Y.; Maharubin, S.; Tan, G. Z. Microtube-Embedded Microfluidic Devices for Potential Applications in Blood Brain Barrier Research. *Procedia Manuf.*, **2020**, *48*, 294–301. https://doi.org/10.1016/j.promfg.2020.05.050.

[170] Gupta, A.; Patel, V. K.; Kant, R.; Bhattacharya, S. Surface Modification Strategies for Fabrication of Nano-Biodevices: A Critical Review. *Rev. Adhes. Adhes.*, **2016**, *4* (2), 166–191. https://doi.org/10.7569/RAA.2016.097307.

[171] Vilela, D.; Romeo, A.; Sánchez, S. Flexible Sensors for Biomedical Technology. *Lab Chip*, **2016**, *16* (3), 402–408. https://doi.org/10.1039/c5lc90136g.

[172] Dashtaki, N. J. M.; Nassajpour-Esfahani, A. H.; Bayareh, M.; Rezai, P.; Doostmohammadi, A. Highly Conductive Multi-Walled Carbon Nanotube/Polydimethylsiloxane (MWCNT/PDMS) Nanocomposite for Microfluidic Applications. *J. Compos. Mater.*, **2020**. https://doi.org/10.1177/0021998320977643.

[173] Bonyár, A.; Izsold, Z.; Borók, A.; Csarnovics, I.; Himics, L.; Veres, M.; Harsányi, G. PDMS-

Au/Ag Nanocomposite Films as Highly Sensitive SERS Substrates. *Proceedings*, **2018**, *2* (13), 1060. https://doi.org/10.3390/proceedings2131060.

[174] Wu, D.; Wei, M.; Li, R.; Xiao, T.; Gong, S.; Xiao, Z.; Zhu, Z. A Percolation Network Model to Predict the Electrical Property of Flexible CNT / PDMS Composite Films Fabricated by Spin Coating Technique. **2019**, *174* (March). https://doi.org/10.1016/j.compositesb.2019.107034.

[175] Promsawat, N.; Promsawat, M.; Janphuang, P.; Luo, Z.; Beeby, S.; Rojviriya, C.; Pakawanit, P.; Pojprapai, S. CNTs-Added PMNT/PDMS Flexible Piezoelectric Nanocomposite for Energy Harvesting Application. *Integr. Ferroelectr.*, **2018**, *187* (1), 70–79. https://doi.org/10.1080/10584587.2018.1445684.

[176] Jang, H. H.; Park, J. S.; Choi, B. Flexible Piezoresistive Pulse Sensor Using Biomimetic PDMS Mold Replicated Negatively from Shark Skin and PEDOT:PSS Thin Film. *Sensors Actuators, A Phys.*, **2019**, *286*, 107–114. https://doi.org/10.1016/j.sna.2018.12.015.

[177] Xu, M.; Gao, Y.; Yu, G.; Lu, C.; Tan, J.; Xuan, F. Flexible Pressure Sensor Using Carbon Nanotube-Wrapped Polydimethylsiloxane Microspheres for Tactile Sensing. *Sensors Actuators, A Phys.*, **2018**, *284*, 260–265. https://doi.org/10.1016/j.sna.2018.10.040.

[178] Majooni, Y.; Mortaheb, H. R.; Khodadadi Dizaji, A. Enhancement in Pervaporative Performance of PDMS Membrane for Separation of Styrene from Wastewater by Hybridizing with Reduced Graphene Oxide. *J. Environ. Manage.*, **2020**, *261* (December 2019), 110189. https://doi.org/10.1016/j.jenvman.2020.110189.

[179] Saharudin, K. A.; Karim, M. A.; Sreekantan, S. Preparation of a Polydimethylsiloxane (PDMS)/Graphene-Based Super-Hydrophobic Coating. *Mater. Today Proc.*, **2019**, *17*, 752–760. https://doi.org/10.1016/j.matpr.2019.06.359.

[180] Bae, J.; Hwang, Y.; Ha, J. H.; Kwon, O. S.; Jang, A.; Kim, H. J.; An, J.; Lee, C. S.; Park, S. H. Versatile Chemical Sensors Using Oligosaccharides on Cleanable PDMS/Graphene Hybrids for Monitoring Environmentally Hazardous Substances. *Appl. Surf. Sci.*, **2020**, *507* (December 2019), 145139. https://doi.org/10.1016/j.apsusc.2019.145139.

[181] Basu, M.; Parihar, V.; Lincon, A.; Joshi, V. P.; Das, S.; DasGupta, S. Development of Graphene Oxide – PDMS Composite Dielectric for Rapid Droplet Movement in Digital Microfluidic Applications. *Chem. Eng. Sci.*, **2021**, *230*, 116175. https://doi.org/10.1016/j.ces.2020.116175.

[182] Oh, J. H.; Woo, J. Y.; Jo, S.; Han, C. S. Pressure-Conductive Rubber Sensor Based on Liquid-Metal-PDMS Composite. *Sensors Actuators, A Phys.*, **2019**, *299*, 111610. https://doi.org/10.1016/j.sna.2019.111610.

[183] Gupta, A.; Geeta, B.; Bhattacharya, S. Novel Dipstick Model for Portable Bio-Sensing Application. *J. Energy Environ. Sustain.*, **2019**, *7*, 36–41. https://doi.org/10.47469/JEES.2019.V07.100075.

[184] Memon, F.; Mukherji, S. CNT/CB-PDMS Nanocomposite Diaphragm Pressure Sensor for Monitoring Respiratory Disorder. *Proc. IEEE Conf. Nanotechnol.*, **2019**, *2018-July*, 1–2. https://doi.org/10.1109/NANO.2018.8626357.

[185] Zhai, W.; Xia, Q.; Zhou, K.; Yue, X.; Ren, M.; Zheng, G. Multifunctional Flexible Carbon Black /

Polydimethylsiloxane Piezoresistive Sensor with Ultrahigh Linear Range , Excellent Durability and Oil / Water Separation Capability. *Chem. Eng. J.*, **2019**, *372* (January), 373–382. https://doi.org/10.1016/j.cej.2019.04.142.